NON-LINEAR ABSORPTION AND PHOTOTHERMAL STUDIES ON ZnO QUANTUM DOTS SYNTHESIZED THROUGH SOL-GEL METHOD

PROJECT REPORT

Submitted by

ANN ROSE P

Register Number: AM21PHY005

Under the guidance of

Dr. SANTHI A, Assistant professor

Department of Physics, St. Teresa's College (Autonomous), Ernakulam.

Kochi- 682011

Submitted to

Mahatma Gandhi University, Kottayam

In partial fulfillment of the requirements for the award of the degree of

MASTER OF SCIENCE

In

PHYSICS

DEPARTMENT OF PHYSICS

ST. TERESA'S COLLEGE (AUTONOMOUS)

ERNAKULAM

ST. TERESA'S COLLEGE
(AUTONOMOUS)
ESTD 1925

CERTIFICATE

This is to certify that the project report entitled **'NON-LINEAR ABSORPTION AND PHOTOTHERMAL STUDIES ON ZnO QUANTUM DOTS SYNTHESIZED THROUGH SOL-GEL METHOD'** is an authentic work done by ANN ROSE P, St. Teresa's college, Ernakulam, under my supervision at department of physics, St. Teresa's college for the partial requirements for the award of Master of Science in Physics during the academic year 2022-23. The work presented in this dissertation has not been submitted for any other degree in this or any other university.

Supervising guide
Dr. SANTHI A.
Assistant professor

Head of the Department
Dr. PRIYA PARVATHI AMEENA JOSE
Assistant professor

PLACE: Ernakulam

DATE: 7.6.23

ST. TERESA'S COLLEGE (AUTONOMOUS)

ERNAKULAM

M.Sc. PHYSICS

PROJECT REPORT

Name : ANN ROSE P

Register Number : AM21PHY005

Year of Work : 2022-2023

This is to certify that this project work entitled **'NON-LINEAR ABSORPTION AND PHOTOTHERMAL STUDIES ON ZnO QUANTUM DOTS SYNTHESIZED THROUGH SOL-GEL METHOD'** is an authentic work done by ANN ROSE P.

Staff member in-charge
Dr. SANTHI A.

Head of the Department
Dr. PRIYA PARVATHI AMEENA JOSE

Submitted for the university examination held at St. Teresa's College, Ernakulam.

DATE: 7.6.2023

EXAMINERS:
1. Dr. REKHA. S
2. Dr. Louie Fribel P G

Department of Physics St. Teresa's College (Autonomous) Ernakulam

ST.TERESA'S COLLEGE (AUTONOMOUS) ERNAKULAM

Certificate of Plagiarism Check for Thesis

Author Name	ANN ROSE P
Course of Study	MSc. PHYSICS
Name of Guide	Dr. SANTHI A.
Department	Physics & Centre For Research
Acceptable Maximum Limit	20%
Submitted By	library@teresas.ac.in
Paper Title	NON-LINEAR ABSORPTION AND PHOTOTHERMAL STUDIES ON ZnO QUANTUM DOTS SYNTHESIZED THROUGH SOL-GEL METHOD
Similarity	0%
Paper ID	757059
Submission Date	2023-05-30 16:15:36

Signature of Student

Signature of Guide

Checked By
College Librarian

* This report has been generated by DrillBit Anti-Plagiarism Software

DECLARATION

I, **ANN ROSE P**, final year M.Sc. Physics student, Department of Physics, St. Teresa's College, Ernakulam, do hereby declare that the project work entitled '**NON-LINEAR ABSORPTION AND PHOTOTHERMAL STUDIES OF ZnO QUANTUM DOTS SYNTHESIZED THROUGH SOL-GEL METHOD**' has been originally carried out under the guidance and supervision of Dr. SANTHI A., Assistant Professor, Department of Physics, St. Teresa's College (Autonomous), Ernakulam in partial fulfilment for the award of the degree of Master of Physics. I further declare that this project is not partially or wholly submitted for any other purpose and the data included in the project is collected from various sources and are true to the best of my knowledge.

Ann Rose P

PLACE: Ernakulam

DATE: 7.6.2023

ACKNOWLEDGEMENT

I express my sincere gratitude to all those who helped me to achieve the moment of satisfaction. First, I thank the lord almighty for the immense grace at every stage of the project. I am highly indebted to my project guide Dr. Santhi A., Assistant Professor, Department of Physics, St. Teresa's College, Ernakulam for her valuable guidance and constant supervision as well as for providing necessary information regarding the project.

I owe much thanks to our teachers, Dr. Frincy Francis, who was there to support us throughout the project sparing her valuable time, and Ms. Minu Pius, for her valuable suggestions.

I would like to express my gratitude to all the staff members of the Physics Department, St. Teresa's college, for their valuable guidance and suggestions for completing the project and for all those who have willingly helped me out of their abilities.

PUBLISHED WORKS

[1] **P. Ann Rose**, Amala Shajan, Francy Francis, M.U. Farzana, Minu Pius, Santhi Ani Joseph, "Studies on thermal diffusion of Aqueous solution of Zinc oxide (ZnO) microtubes in gold (Au) using dual beam thermal lens experiment", Materials Today:Proceedings,2023.

https://doi.org/10.1016/j.matpr.2023.05.135

Contents lists available at ScienceDirect

Materials Today: Proceedings

journal homepage: www.elsevier.com/locate/matpr

Studies on thermal diffusion of Aqueous solution of Zinc oxide (ZnO) microtubes in gold (Au) using dual beam thermal lens experiment

Ann Rose P. *, Amala Shajan, Francy Francis, Farzana M.U., Minu Pius, Santhi Ani Joseph

Department of Physics and Centre for Research, St. Teresa's College, Ernakulam PIN 682011, India

ARTICLE INFO

Article history:
Available online xxxx

Keywords:
Thermal Diffusivity
ZnO microtube
Gold nanosol
Dual beam thermal lens experiment

ABSTRACT

This work reports the anomalous enhanced thermal diffusivity of hybrid nanofluid of ZnO microtubes in Au nanosol determined using a dual beam thermal lens experiment. ZnO microtubes were synthesised using the low-temperature hydrothermal method and Au nanoparticles were prepared by the Turkevich method. The hybrid fluid was prepared using the two step method.The thermal diffusivity for different volume fractions (0 to 14%) for various molarities of ZnO(0.03 M,0.05 M,0.07 M) in Au nanosol was obtained. The results obtained reveal optimum molarity of 0.05 M of ZnO and an optimum volume fraction which enhances thermal diffusivity.

Selection and peer-review under responsibility of the scientific committee of the 2nd International Conference on Multifunctional Materials.

1. Introduction

Zinc oxide is a metal oxide semiconductor which has received special attention owing to it's electrical, optical and magnetic properties among many others, which gives them a large potential for various applications in optoelectronics [1]. Zinc oxide is popular for its large band gap (3.37 eV), significant exciton binding energy 60 meV and wide optoelectronic applications. It portrays peculiar properties such as non-toxicity, high sensitivity, bio-

ation of the energy absorbed from the pump laser. The present study of thermal diffusivity of ZnO-Au nanofluid aims to mark its uncompromised application in biomedical researches which requires the material to have desired thermal properties along with being biocompatible.

2. Sample preparation

The hybrid nanofluid of ZnO microtubes with Au nanoparticles

PAPERS PRESENTED IN INTERNATIONAL AND NATIONAL CONFERENCES

[1] Ann Rose P., Amala Shajan, Frincy Francis, M.U. Farzana, Minu Pius, Santhi Ani Joseph, “Studies on thermal diffusion of Aqueous solution of Zinc oxide (ZnO) microtubes in gold (Au) using dual beam thermal lens experiment", 2nd International Conference on Multifunctional Materials-2022, 12102.

[2] Ann Rose P, Amala Shajan, Frincy Francis, Merin Joby, Meera Venugopal, Ani Joseph Santhi, “Nonlinear Absorption and Photothermal Studies on Chemically Synthesised ZnO Quantum Dots”, Poster presentation - Annual Physics Symposium, Department of Physics and Centre for Research, St. Teresa’s College, Ernakulam PIN 682011, India, 2023

[3] Ann Rose P, Amala Shajan, Frincy Francis, Merin Joby, Meera Venugopal, Ani Joseph Santhi, “Nonlinear Absorption and Photothermal Studies on Chemically Synthesised ZnO Quantum Dots”,Scientia 2023, Department of Chemistry and Centre for Research, St. Teresa’s College, Ernakulam PIN 682011, India.

NON-LINEAR ABSORPTION AND PHOTOTHERMAL STUDIES OF ZnO QUANTUM DOTS SYNTHESIZED THROUGH SOL-GEL METHOD

ABSTRACT

This work is in the realm of Nanotechnology, and investigates the thermo-optic and non-linear properties of Zinc Oxide Quantum Dots, thus determining its role in various optoelectronic applications. Zinc Oxide Quantum Dots were prepared using a versatile route related to the Sol-gel process, at three different pH values, and were characterized using X-ray Diffraction, HR-TEM, FTIR, Absorption and Photoluminescence studies. Thermal Diffusivity of the prepared samples were investigated using Dual Beam Thermal Lens Experiment, and Non-Linear Absorption was studied by employing the Open Aperture Z-Scan Technique.

CONTENTS

Table of Contents

Chapter 1

INTRODUCTION

"There is plenty of room at the bottom"

- Richard Feynman

Nanoscience and nanotechnology have opened a plethora of exciting opportunities in diverse fields. Properties of materials get modified at nano regime. The electrons and holes experience quantum confinement and this leads to changes in physical, optical, chemical, electrical and magnetic properties during the transition from bulk to the quantum confined structures. Technologies are being developed to exploit these changes to be applied in fields such as nanophysics, nano chemistry, nanobiotechnology, nanomedicine, nano photonics and many more.

1.1. Quantum Dots

Quantum Dots are referred to as the 0-DEG system. Electrons and holes experience restriction in motion in all three dimensions of spatial configuration. In other words, when it comes to QDs the delocalization dimension is 0 and localization dimension is 3. Since QDs are analogous to the case when an electron is confined in a three-dimensional electron gas model, these nano-structures exhibit complete set of different properties when compared to higher dimensioned structures. QDs are similar to atoms, with respect to the presence of discrete energy levels as well as the and the spatial confinement experienced by both.

Density of states D(E) with energy of QDs is a set of discrete lines indicating larger number of energy states at a particular value of energy. This modification in the pattern of density of states has been known to be the reason for sharp absorption and emission spectra of these lower dimensioned structures. Increased number of energy levels at a given energy spacing would mean there is increased chance for excitation and deexcitation owing larger population that can be accommodated in these levels. The absorption and emission spectra of QDs are sharp and discrete similar to the D(E).

At lower dimension structures, the gap between lowest conduction and highest valence is increased. This phenomenon is referred to as the ‘blue shift ‘in band gap. Hence band gap of QDs is much higher than that of the corresponding bulk structure.

1.2. ZnO QDs

ZnO QDs belong to the category of semiconducting quantum dots, hence has a wide range of applications in fields of science, engineering and technology. It is well known as a tunable material with respect to its strong emissive behavior, when compared to organic fluorescent molecules. In contrast to the conventionally used Cd –based chalcogenides QDs, which is toxic for many biomedical applications, ZnO QDs is well known for its biocompatible nature.

ZnO is a direct bandgap semiconductor with bandgap energy of 3.37eV. It is popular for its adaptive nature, tunability, biocompatibility, nontoxicity and large exciton binding energy of 60meV which makes it a huge potential applicant in optoelectronic devices, biosensors, photonic devices, gas sensors, solar cells etc. High absorption coefficient, ease of doping, good carrier mobility and versatile synthesis conditions for producing various geometries of ZnO nanoparticles makes it an interesting research material.

1.3. Various synthesis techniques

Synthesis techniques can be classified as bottom up and top-down approaches depending how the nanostructures are built. Bottom-up technique involves building up nanostructures by individually assembling the component atoms or molecules. On the other hand, when nanostructures are built by fragmenting a bulk material, the approach is referred to as top-down synthesis techniques. Physical Vapor Deposition, Chemical Vapor Deposition, Molecular Beam Epitaxy, Wet Chemical, Pulsed Laser Deposition are well known examples for Bottom-up approaches. Nano-lithography, Ball-milling techniques come under top-down methods of synthesis.

ZnO QDs are commonly synthesized using chemical methods. Some of the approaches undertaken are discussed below:

(i) **From biological extracts**:

ZnO QDs can be prepared from *Coriandrum sativum.* The leaves of Coriandrum sativum are cleaned thoroughly to remove unwanted dirt and impurities. A given quantity of these leaves is mixed with ethanol and heated to about 80°C for about half an hour. The resulting mixture

is cooled to room temperature and filtered. An equal quantity of zinc acetate dihydrate is added to this extract, followed by the addition of NaOH under constant stirring to increase the pH of the solution and to induce precipitation. A color change from brown to yellowish white can be observed. This is then washed several times with ethanol to remove unreacted molecules and calcinated at 400°C to obtain the yellowish white precipitate.

(ii) **Sol-gel method**

Separate solutions of zinc acetate dihydrate and KOH were prepared in ethanol and mixed at 60°C under constant stirring. The solution was then cooled down to room temperature, centrifuged and washed several times with ethanol and dried.

Research works are being undertaken to exploit unique properties to the fullest. Studies on synthesizing stabilized solution of aqueous dispersion of ZnO QDs which show strong blue emissions are being carried out. There are successful investigations of aqueous dispersion of ZnO QDs of various sizes showing luminescence in visible region.

The present study focuses on the thermo-optic characterization of ZnO QDs with Silica capping prepared using the intermediate sol gel technique. Structural, optical and morphological characterizations were done to confirm the formation of ZnO QDs of pH 10,12 and 14. Dual beam thermal lens technique is employed to investigate the thermal diffusivity of the sample and to explore the thermal diffusion behavior at various volume fractions to find out its application as coolant in various devices and also in biomedical applications where it is necessary to trap heat at a localized point for treatment and curing of certain diseases. Non-linear optical studies are carried out to probe its potential in applications such as in passive mode-locking, Q-switching and as optical limiters.

Chapter 2

SYNTHESIS OF ZINC OXIDE QUANTUM DOTS

2.1. Conventional Sol-gel methods

Solgel method is the most common synthesis technique used for the preparation of Zinc Oxide Quantum Dots. Solgel methods are broadly classified into two.

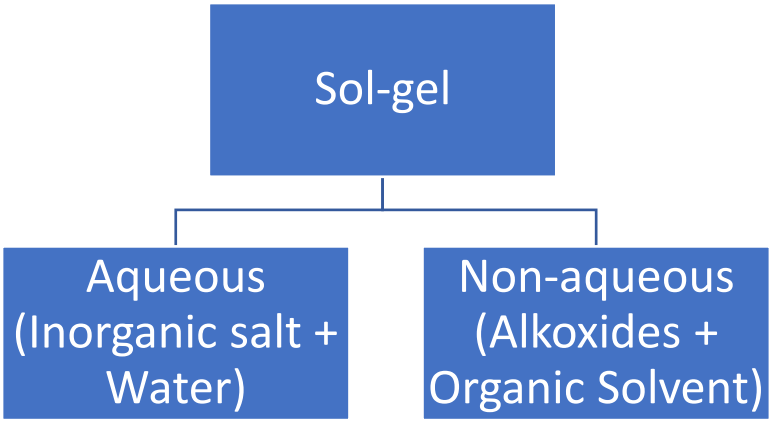

Figure 2. 1 Classification of sol-gel method

Aqueous sol-gel methods involve Inorganic salts containing the required metal cation, such as Zinc Acetate, Zinc Chloride, Zinc Sulfate etc, dissolved in water. The process is usually carried out at high temperatures. Non-aqueous sol-gel methods involve alkoxides of the required metal, such as Zinc Dimethoxide, Zinc Diethoxide etc, dissolved in organic solvents. These methods have better reaction control at the atomic scale, but the alkoxides are hard to procure. This is due to their polymeric and water-insoluble nature, which makes their synthesis procedures harder, and not commercially available with ease.

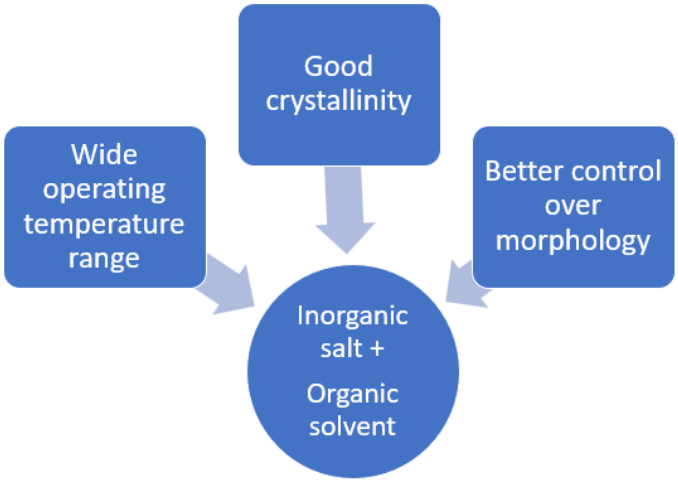

Figure 2. 2 The intermediate sol-gel method

2.2. An Intermediate route to Sol-gel Method

Here, we overcome the disadvantages of the conventional sol-gel methods by going for an intermediate sol-gel method, where an inorganic salt is dissolved in an organic solvent. This method retains the benefit of non-aqueous method, along with gaining an added advantage of a wide operating temperature range, which makes synthesis at room temperature possible. The samples prepared by this intermediate solgel method were also found to have good crystallinity and better control over morphology.

Here, the chosen inorganic salt is Zinc Acetate and the organic solvent taken is Methanol. 0.1 M Zinc Acetate solution and 1 M Potassium Hydroxide solution were taken as the precursors. Zinc Acetate Solution was prepared by dissolving 0.55 g of Zinc Acetate Dihydrate (*98.5% purity, Nice Chemicals (P) Ltd.*) in 25ml of Methanol, and Potassium Hydroxide solution was prepared by dissolving 2.8 g of Potassium Hydroxide pellets (*Spectrum Reagents and Chemicals Pvt. Ltd.*) in 50 ml of Methanol. Both solutions were magnetically stirred for 10 minutes each.

Zinc Acetate solution was taken in a beaker and kept on a magnetic stirrer along with a digital pH meter arrangement at room temperature. The setup is shown in figure 2.3.

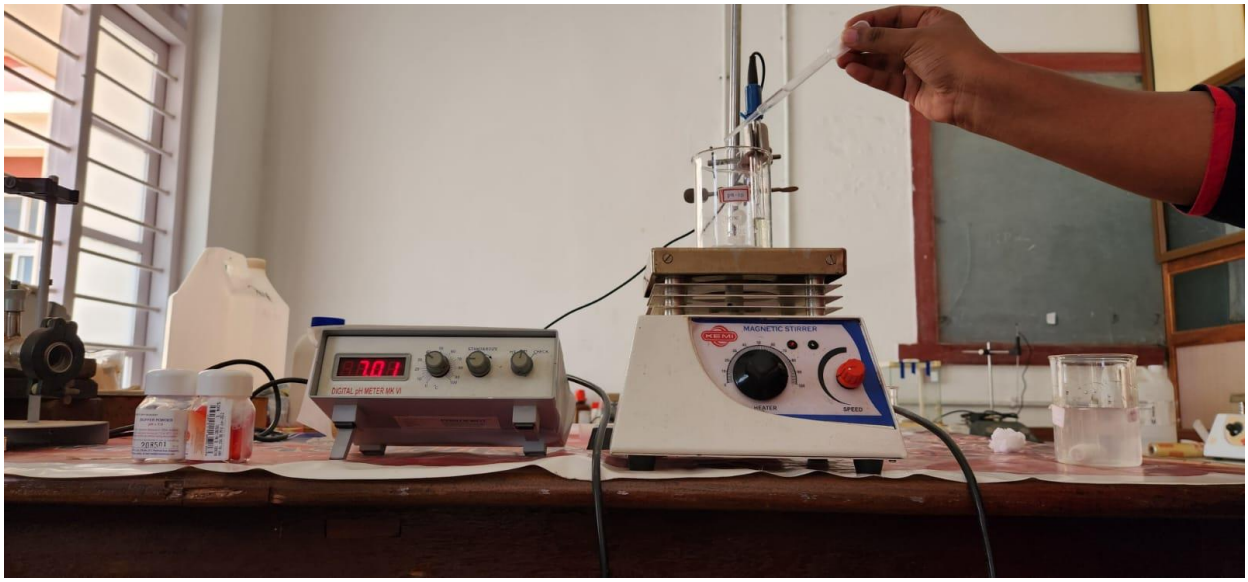

Figure 2. 3 Magnetic stirrer and pH meter setup

The digital pH meter was calibrated using buffer solutions of pH values 4 and 7. Potassium Hydroxide solution was added dropwise into the Zinc Acetate solution with constant stirring and pH value was being continuously monitored. The solution which was initially acidic, recorded rise in pH value on addition of the alkaline Potassium Hydroxide Solution. The addition of Potassium Hydroxide was continued until the required pH value-10 was obtained. The solution was then taken out from the arrangement and homogenized by magnetic stirring for 1 hour. The formation of ZnO quantum dots were confirmed using different characterization techniques.

The corresponding chemical reaction equation is as follows:

$$Zn(CH_3COO)_2 + 2\ KOH \rightarrow ZnO + H_2O + 2\ CH_3COOK$$

0.25 ml of Tetraethyl Orthosilicate (TEOS) solution (*reagent grade 98%, Sigma-Aldrich*) was added into the homogenized solution to prevent agglomeration of the nanoparticles. Further, 0.5 ml of water was added to the solution to enable mild sol-gel reaction of TEOS on the particle surfaces. The colloidal ZnO solution thus prepared was separated by centrifuging at 6000 rpm for 60 minutes, and washing with methanol for several times and then with water to remove all the unreacted particles. The centrifuging and washing were repeated in three steps.

Figure 2. 4 Tetraethyl Orthosilicate

Figure 2. 5 Laboratory centrifuge set at 6000 rpm for 60 mins

After the final centrifugation, the supernatant part of the sample was set aside for further investigation, as the Quantum Dots are ideally found in the supernatant part. This sample will be mentioned as S1 for convenience . The portion settled in the bottom of the tubes were redispersed in water to prepare the ZnO quantum dots colloidal solution of pH 10.

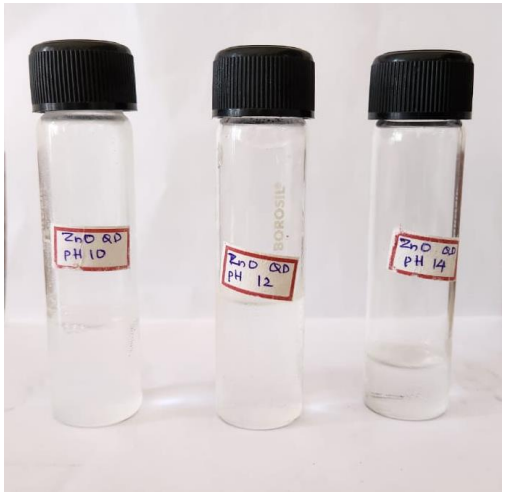

Figure 2. 6 ZnO Quantum Dots Colloidal solutions of pH 10,12 and 14

The same procedure is repeated to synthesize ZnO quantum dots colloidal solution of pH 12 and 14 (figure 2.6). The colloidal samples were further dried in sunlight and grinded using a mortar and pestle and was used for X-ray diffraction and FTIR studies.

The powdered sample, which we'll mention by S2, was further redispersed in water for the Optical Characterizations, Thermal Diffusivity studies and Non-Linear Optical Studies.

Figure 2. 7 Fine powdered ZnO Quantum Dots

The samples were prepared in three different reaction pH, expecting an increase in the size of the particles, with increase in pH. The effect of pH of the reaction solution on the growth of

the particles has been reported in several papers. The increased concentration of OH^- ions cause the growth and ripening of the particles to be accelerated, thus increasing the particle size.

Table 2. 1 Molarities and required masses of initial precursors

Solution	Solute	Molecular mass of Solute (g/mol)	Mass of Solute (g)	Solvent	Volume of Solvent (ml)	Molarity
Zinc Acetate Solution	Zinc Acetate Dihydrate	219.49	0.55	Methanol	25	0.1 M
Potassium Hydroxide Solution	Potassium Hydroxide	56.10	2.8		50	1 M

Chapter 3

CHARACTERISATIONS

Th evolution of Materials Science over the decades was aided by numerous characterization techniques which were developed to investigate and measure the properties of the materials synthesized by various methods. Modern characterization techniques offer great accuracy in the measurement and analysis of the structure, chemical composition, electrical properties, thermal properties, optical properties etc. of the material.

Here we have employed the following characterization techniques to analyze and confirm the nature of the synthesized sample.

- High Resolution Transmission Electron Microscopy (HR-TEM)
- X-Ray Diffraction (XRD)
- Fourier Transform Infrared Spectroscopy (FTIR)
- UV – Visible Spectroscopy
- Photoluminescence Spectroscopy

3.1. Structural Characterizations

There exists a number of Structural Characterization techniques, that reveal a multitude of information about the various structural properties of the synthesized material. Atomic Force Microscopy reveals the Surface defects, roughness and morphology. Crystalline structure, strain, lattice parameters etc. can be estimated from X-Ray Diffraction. Transmission Electron Microscopy reveals the quality and thickness of the epitaxial layer. These are a few commonly used techniques. Here, our samples are characterized using HR-TEM and XRD.

3.1.1. High Resolution Transmission Electron Microscopy

High Resolution- Transmission Electron Microscopy or HR-TEM is an imaging technique that is similar to conventional microscopy techniques. Where light is used for imaging in conventional microscopes, HR-TEM uses electrons, thus producing high quality images with resolution comparable to that of the De Broglie wavelength of the electron. Unlike Scanning

Electron Microscopy (SEM) which produces three dimensional images, TEM is capable of producing only two-dimensional images. The image is produced by interpreting the electrons transmitted through the sample. The transmitted electrons will have undergone elastic or inelastic scattering with the atoms in the sample, and the elastically scattered electrons are utilized for the imaging. The inelastically scattered electrons are of no use for HR-TEM, but can be utilized for another analysis technique called the Electron Energy Loss Spectroscopy (EELS).

Since HR-TEM enables imaging in the nanoscale, it is much useful in the study of crystals, metals, semiconductors etc., even in identifying their defects in the atomic scale.

Here, the ZnO Quantum Dots Colloidal solutions of pH 10 and pH 14 were analyzed using HR-TEM and the following images were obtained.

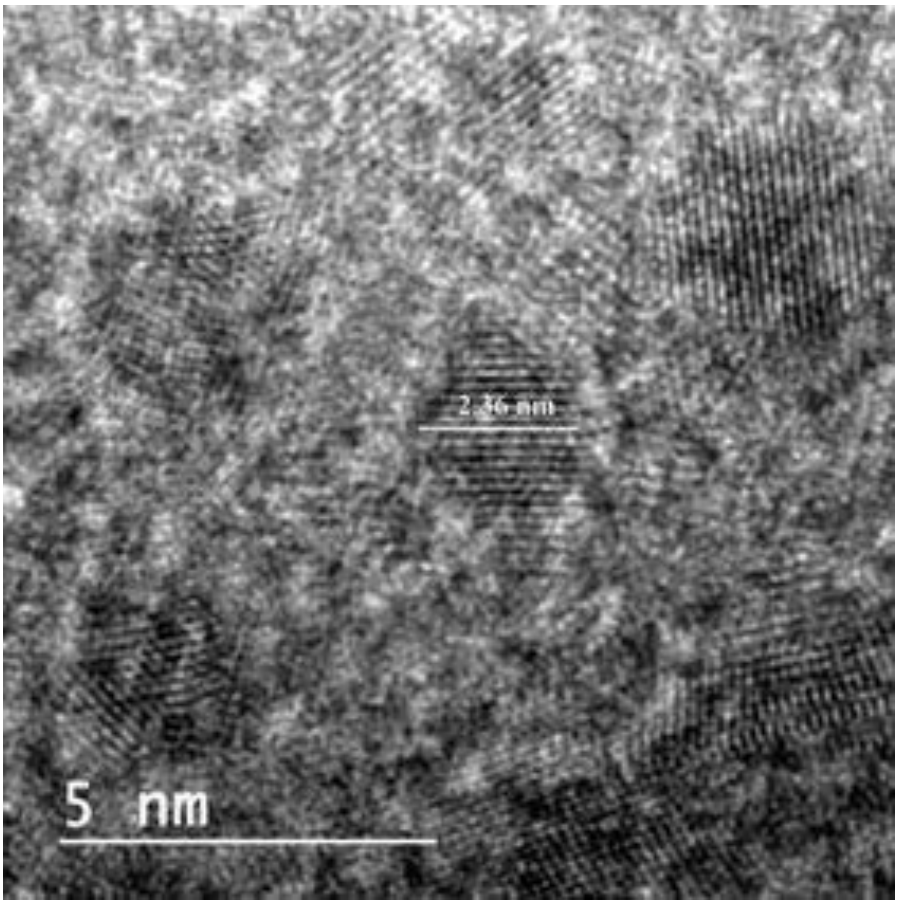

Figure 3. 1 HR-TEM image of pH 10 ZnO QD

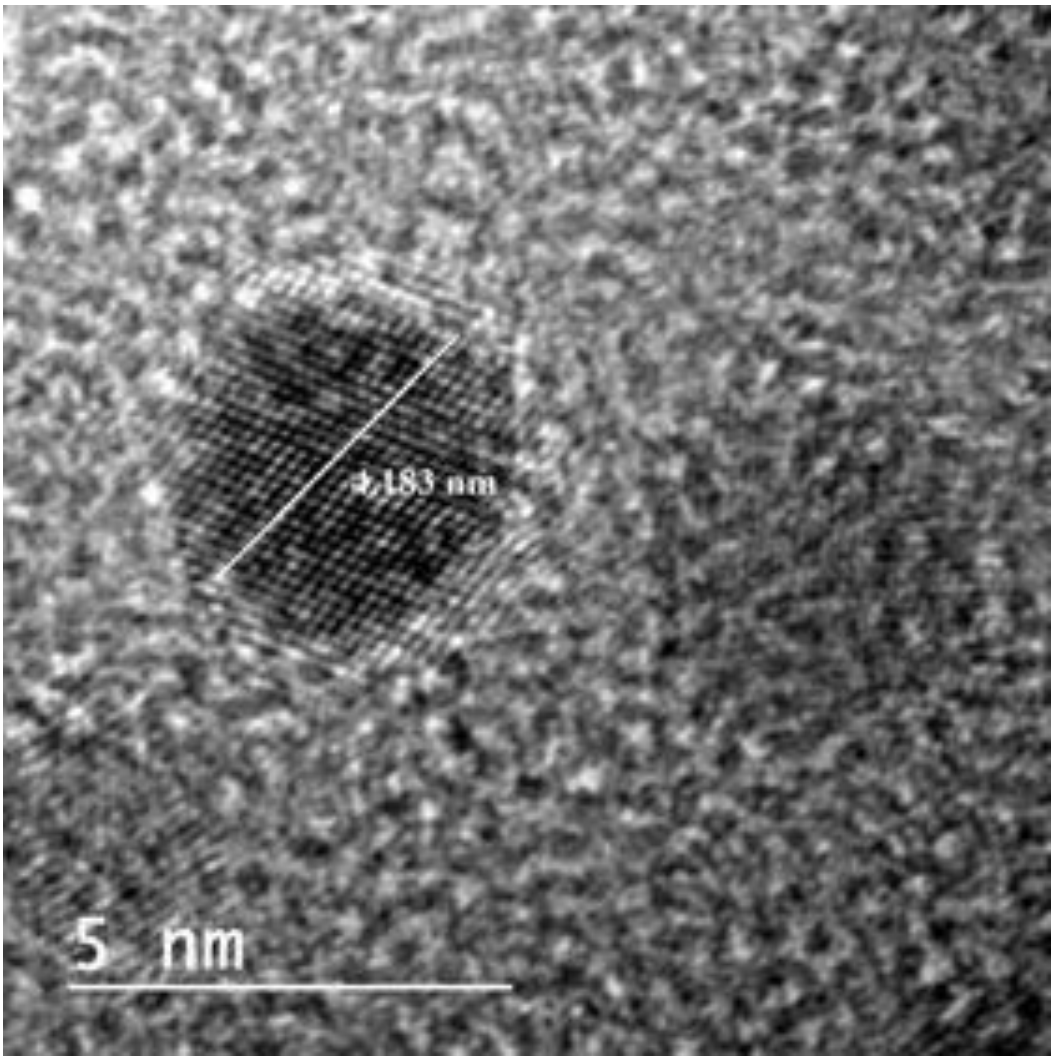

Figure 3. 2 HR-TEM image of pH 14 ZnO QD

Figure 3.1 and Figure 3.2 reveals the ZnO Quantum Dots of pH 10 and pH 14 with spherical structure, and average particle size of 2.36 nm and 4.183 nm respectively, which confirms with our hypothesis of increase in particle size with increase in reaction pH. The reaction takes place between Zinc Acetate Solution and Potassium Hydroxide Solution. An increase in pH simply means an increase in the concentration of OH^- ions, i.e., an increase in the reactant concentration, which in turn increases the growth rate. This causes the concentration of the Zinc Oxide molecules within the solution to increase, and they tend to agglomerate.

The agglomeration of the particles continues until the addition of TEOS. The alkoxyl groups of the TEOS hydrolyze and react with the OH^- ions on the surface of the Zinc Oxide particles, thus forming a layer of Silica around them, effectively stopping any further agglomeration and growth in particle size.

3.1.2. X-Ray Diffraction

X-Ray Diffraction is one of the oldest yet most used characterization technique in Materials Science. X-rays are high energy electromagnetic radiations that are produced when an outer valence electron of an atom transitions to an inner hole. When a crystal is irradiated with an X-ray, the reflected rays from the atomic planes of the crystal interfere to form a diffraction pattern. The interplanar distance d, and the angle of incidence of the X-ray given by θ, are related by the Bragg's Law,

$$2\,d\,sin\,\theta = n\lambda \tag{3.1}$$

Where n is a whole number and λ is the wavelength of the X-ray, which usually is 1.54 Å, which is the wavelength of Kα line of the characteristic waves of Copper.

The Diffraction pattern can be analyzed to deduce the crystal's internal structure. The 2θ values corresponding to the most prominent planes are obtained from the XRD data, which can be used to find the (hkl) values of those planes which are unique to each material. This further confirms the formation of the required crystalline material. The method can also be used to measure the crystal lattice parameters, interplanar spacing, crystallite size, crystal strain, energy density etc.

Here we have used the X-ray Diffraction Technique to mark the (hkl) values of the prominent planes and thereby confirm the ZnO formation, and to measure the crystalline sizes corresponding to each of these planes. Crystallite sizes corresponding to each peak is estimated using the Debye-Scherrer formula

$$D = \frac{k\lambda}{\beta\,cos\,\theta} \tag{3.2}$$

where k is the shape factor, which is usually taken as 0.9 assuming the crystallite to of spherical shape, λ is 1.54Å, β is the Full Width Half Maximum of the peak in radians, and θ is half of the peak position given by 2θ, and Interplanar distance d is found from the Bragg's Law as

$$d = \lambda\,/\,2\,sin\,\theta \tag{3.3}$$

Once we know the values of h,k,l and d, its is easy to find the lattice parameters a and c using the equation,

$$\frac{1}{d^2} = \frac{4}{3}\left[\frac{h^2+hk+k^2}{a^2}\right] + \frac{l^2}{c^2} \tag{3,4}$$

The following XRD patterns were obtained for ZnO Quantum Dots synthesized with reaction pH 10, 12 and 14 respectively (S2).

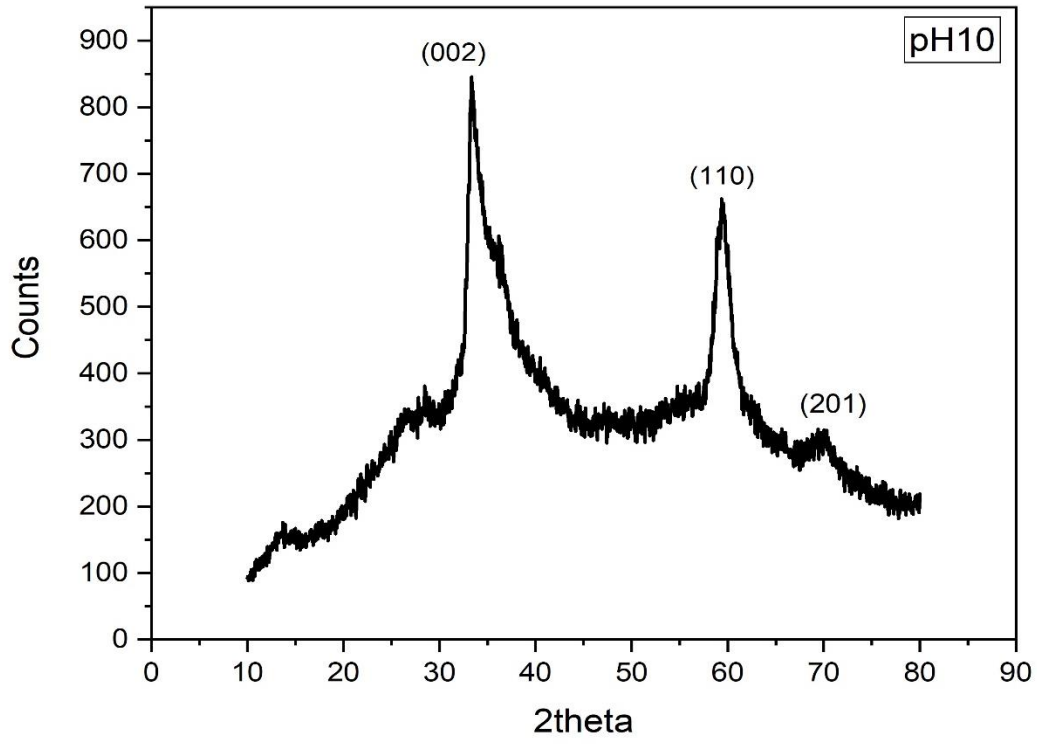

Figure 3. 3 XRD pattern of ZnO Quantum Dots of pH 10

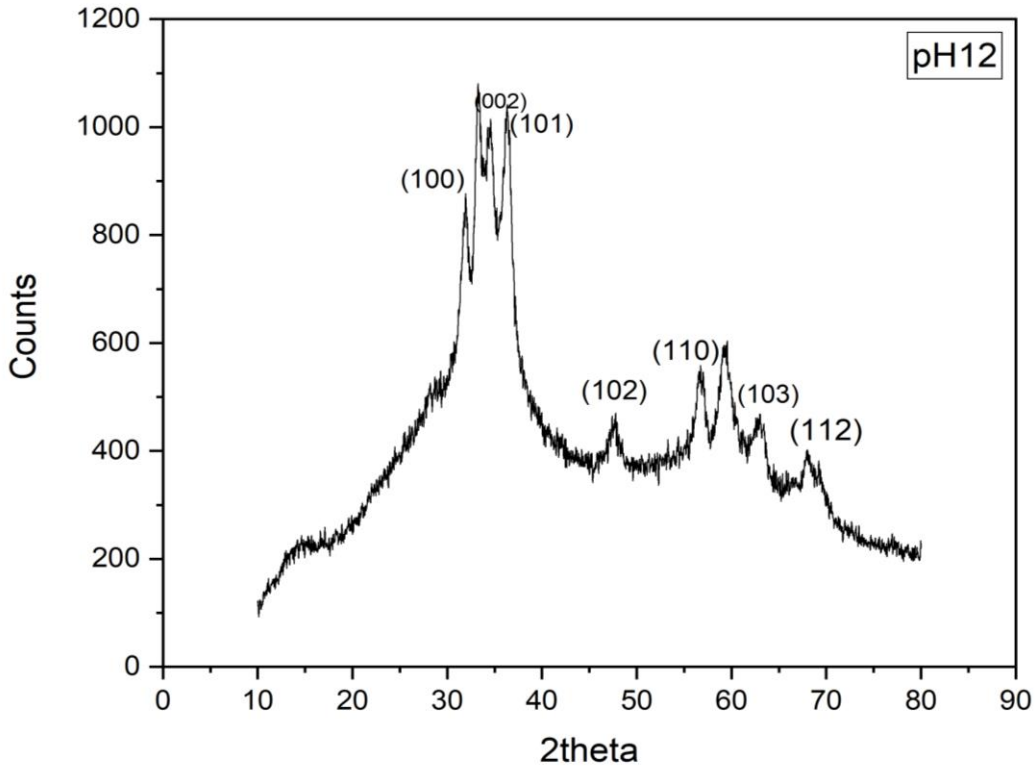

Figure 3. 4 XRD pattern of ZnO Quantum Dots of pH 12

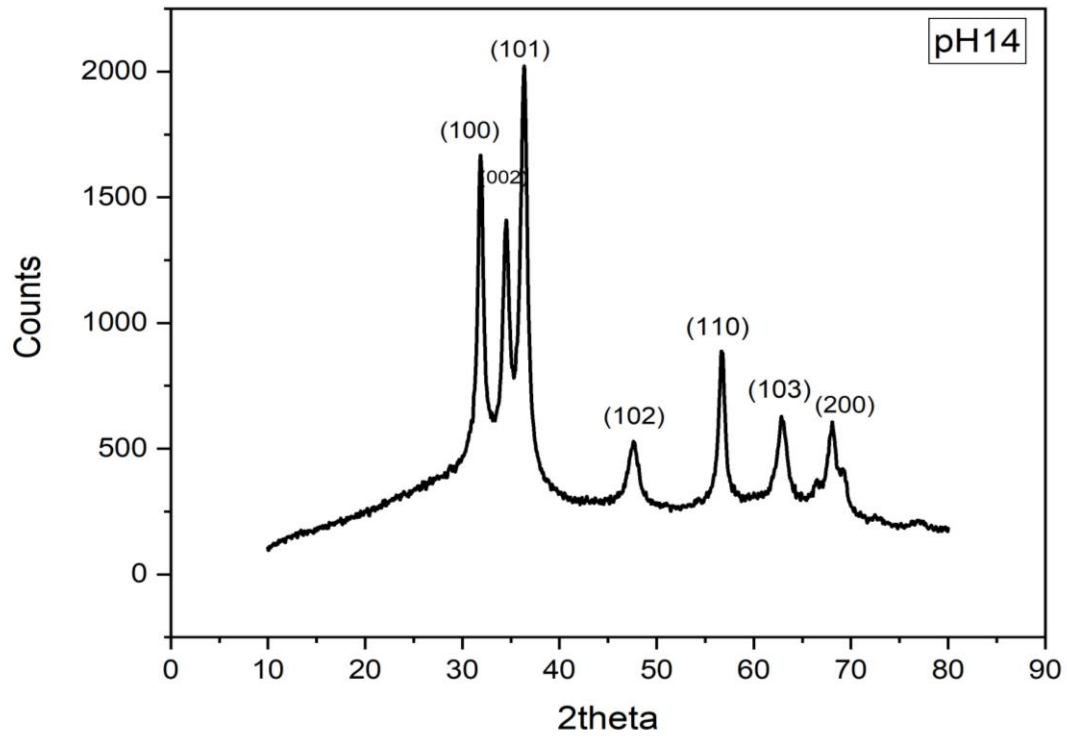

Figure 3. 5 XRD pattern of ZnO Quantum Dots of pH 14

All three XRD patterns show peaks at positions that are in agreement with the standard values 31.64°, 34.43°, 36.29°, 47.75°, 56.51°, 62.90° and 67.98° correscponding to planes with (hkl) values (100), (002), (101), (102), (110), (103) and (112), thus confirming that the sample is Zinc Oxide.

XRD pattern of pH 10 samples are found to have only three peaks with, which could be due to considerable broadening of the peaks due to very small particle sizes, and from the added strain in the system due to necking found between some of the particles in the sample, as evident in the following figure.

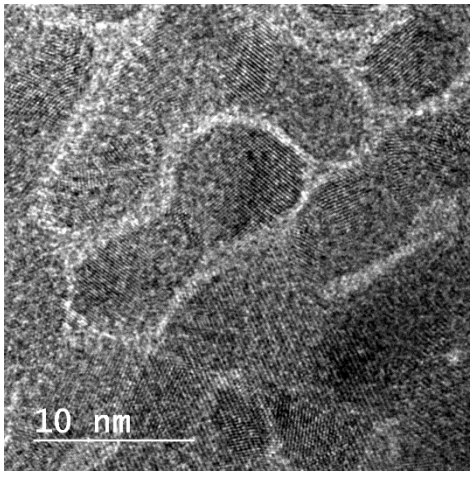

Figure 3. 6 Necking among some Quantum Dots of pH 10

ZnO Quantum Dots of pH 10

The XRD pattern shows three peaks of the seven prominent peaks of Hexagonal Wurtzite ZnO.

The peaks at 34.242°, 57.273° and 69.476° corresponds to the standard peaks at 34.420°, 56.651° and 69.23°, with (hkl) values (002), (110) and (201), thus confirming the sample.

The corresponding crystallite sizes were estimated as shown in the following table using Debye-Scherrer Formula given in equation (3.2)

Table 3. 1 Crystallite sizes in pH 10 ZnO Quantum Dots

Peak positions (2θ) (degrees)	FWHM (β) (radians)	Crystallite size (D) (nm)
34.242	3.105	2.675
57.273	2.020	4.526
69.476	29.676	0.308

The interplanar spacing d in the crystallites corresponding to the above mentioned peaks are as shown in the following table.

Table 3. 2 Interplanar spacings in pH 10 ZnO Quantum Dots

Peak positions (2θ) (degrees)	$d = \lambda / 2 \sin\theta$ (nm)
34.242	0.261
57.273	0.160
69.476	0.135

ZnO Quantum Dots of pH 12

The XRD pattern shows all the seven prominent peaks of Hexagonal Wurtzite ZnO.

The peaks are positioned at 31.524°, 34.925°, 36.419°, 48.294°, 58.455°, 62.526° and 68.526° which corresponds to the standard peaks with (hkl) values (100), (002), (101), (102), (110), (103) and (112), thus confirming the sample.

The corresponding crystallite sizes were estimated as shown in the following table using Debye-Scherrer Formula given in equation (3.2)

Table 3. 3 Crystallite sizes in pH 12 ZnO Quantum Dots

Peak positions (2θ) (degrees)	FWHM (β) (radians)	Crystallite size (D) (nm)
31.524	20.745	3.977
34.925	4.101	20.295
36.419	0.920	90.813
48.294	5.959	14.602
58.455	10.607	8.578
62.526	23.595	3.937
68.526	3.098	31.009

The interplanar spacing d in the crystallites corresponding to the above mentioned peaks are as shown in the following table.

Table 3. 4 Interplanar spacings in pH 10 ZnO Quantum Dots

Peak positions (2θ) (degrees)	$d = \lambda / 2 \sin\theta$ (nm)
31.524	0.283
34.925	0.256
36.419	0.246
48.294	0.188
58.455	0.157
62.526	0.148
68.526	0.136

ZnO Quantum Dots of pH 14

The XRD pattern shows all the seven prominent peaks of Hexagonal Wurtzite ZnO.

The peaks are positioned at 31.880°, 34.498°, 36.356°, 47.580°, 56.704°, 62.887° and 68.077° corresponds to the standard peaks with (hkl) values (100), (002), (101), (102), (110), (103) and (200), thus confirming the sample.

The corresponding crystallite sizes were estimated as shown in the following table using Debye-Scherrer Formula given in equation (3.2)

Table 3. 5 Crystallite sizes in pH 14 ZnO Quantum Dots

Peak positions (2θ) (degrees)	FWHM (β) (radians)	Crystallite size (D) (nm)
31.880	1.385	5.961
34.498	1.470	5.654
36.356	1.058	7.899
47.580	1.552	5.590
56.704	0.945	9.542
62.887	1.626	5.722
68.077	2.089	4.587

The interplanar spacing d in the crystallites corresponding to the above mentioned peaks are as shown in the following table.

Table 3. 6 Interplanar spacings in pH 10 ZnO Quantum Dots

Peak positions (2θ) (degrees)	$d = \lambda / 2 \sin\theta$ (nm)
31.880	0.280
34.498	0.259
36.356	0.246
47.580	0.190
56.704	0.162
62.887	0.147
68.077	0.137

Once we have the values of interplanar spacing d and (hkl), the lattice parameters are estimated by solving equation (3.4) and the following values are obtained..

Table 3. 7 Lattice parameters of ZnO Quantum Dots

Sample	**Interplanar spacing d (angstrom)**	**d_{jcpds} (angstrom)**	**Lattice parameters (angstrom)**	**Lattice parameters (Standard)**	**Aspect Ratio c/a**
pH10 ZnO QD	2.616	2.47	a=b=3.104 c=6.040 $\alpha=\beta=90^0,\gamma=120^o$	a=b=3.25 c=5.206	1.94
pH 12 ZnO QD	2.464		a=b=3.154 c=5.689 $\alpha=\beta=90^0,\gamma=120^o$		1.80
pH 14 ZnO QD	2.469		a=b=3.23 c=6.072 $\alpha=\beta=90^0,\gamma=120^o$		1.87

The lattice parameters calculated from the XRD data are in good agreement with the standard values a=b= 3.25 Å , c= 5.206 Å, and the aspect ratios are found to be close to the ideal aspect ratio for Zinc Oxide, which is 1.6.

The supernatant part of the centrifuged samples were also send for X-Ray Diffraction, since the Quantum Dots could also be possibly found in that part due to them being very light. The XRD data of the supernatant parts(S1) were as follows

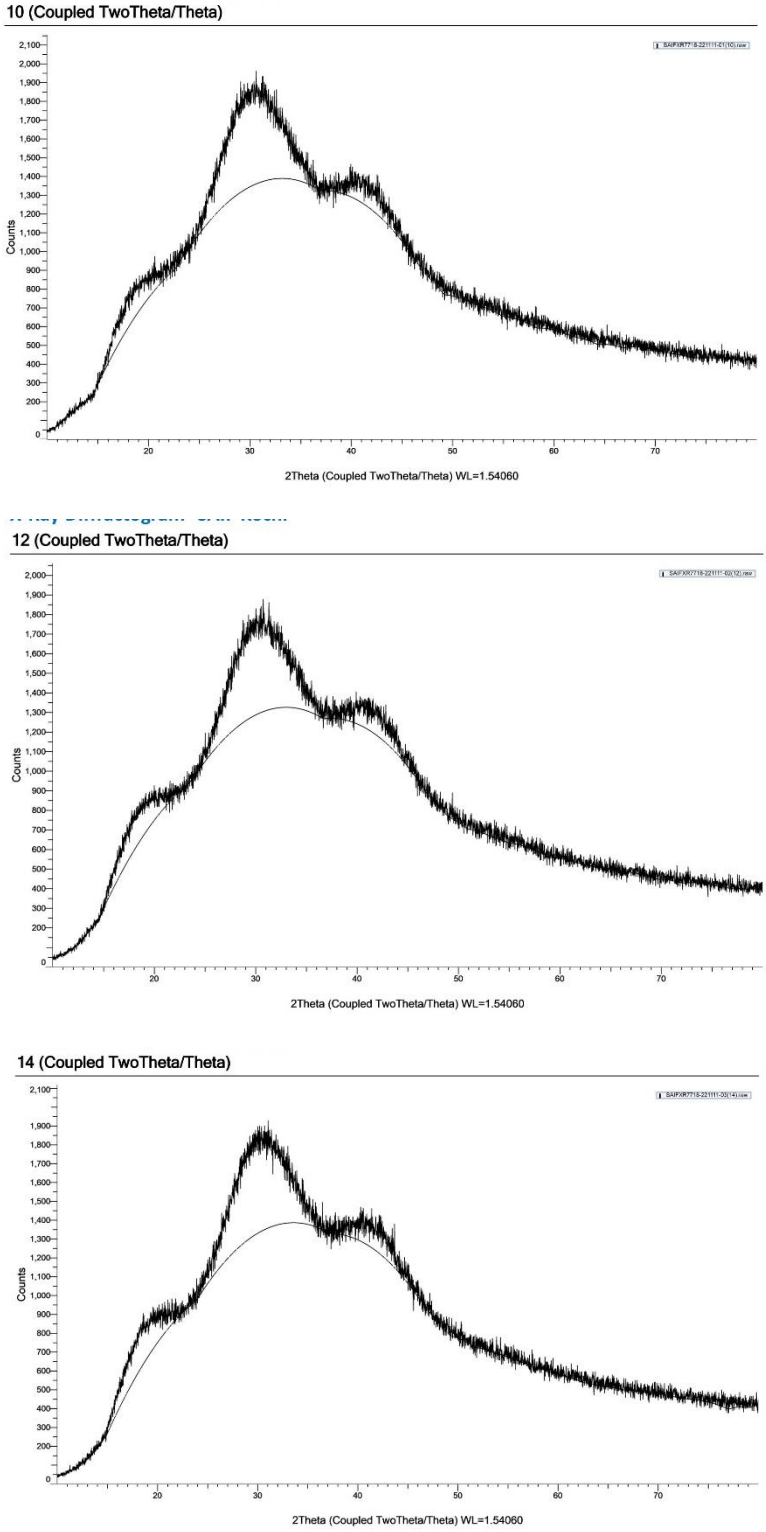

Figure 3. 7 XRD patterns of sample S1 of pH (a) 10 (b) 12 (c) 14

The XRD data reveals the amorphous nature of the supernatant part of the sample, which is attributed to the Silica capping around the particles.

3.2. Optical Characterizations

Optical characterization techniques are non-destructive characterization techniques that use light or photons of electromagnetic radiations to probe the properties of different materials. We can infer ideas on the structure, morphology, physical, chemical and electronic properties of materials from their associated optical properties, thus widening the scope of Optical Characterizations in Materials Science. UV-Vis-NIR Spectrophotometry, Fourier Transform InfraRed Spectroscopy, Ellipsometry etc. are a few examples of Optical Characterizations.

Here, the three samples were characterized using UV-Vis Spectrophotometry, Fourier Transform Infra Red Spectroscopy and Photoluminescence Spectroscopy

3.2.1. Fourier Transform Infrared Spectroscopy

Fourier Transform Infrared Spectroscopy is a great tool for measurements in the mid and far Infrared regions of the Electromagnetic Spectrum. Electromagnetic radiations in IR range interacts mostly with vibrations and rotations of the molecules, which depends on the molecular structure of the material. Thus it is a great tool to probe atomic and molecular structures of materials.

Symmetric vibration modes do not cause absorption in FTIR as it requires a change in dipole moment of the molecule. However, these vibrations will be Raman Active, as being Raman Active requires only a change in Polarizability. Thus, FTIR and Raman Spectroscopy are complementary to each other. IR spectrums are unique for each material and serves as their fingerprints. Thus, the method can be used for identifying unknown materials and confirming known materials.

Zinc Oxide Quantum Dots of pH 14 (S2) were analyzed using FTIR Spectroscopy and the FTIR Spectrum is given in Figure 3.8.

A strong and broad dip in transmission in the 3000 cm^{-1} to 3500 cm^{-1}, is due to O-H stretching vibrations, which is present in almost all the materials.

Two weak dips in transmission due to C=C stretching and O-H bending are also observed, which could be due to the presence of remnants of unreacted organic solvents and salts.

The region from 0 to 1500 cm^{-1} is known as the fingerprint region of the sample, which is unique for each material and helps is identifying the unknown material or confirming the known material.

The fingerprint region has a strong dip about 1000 cm^{-1} due to the C-O stretching vibrations which could be due to remnants of Potassium Acetate which is a byproduct in the reaction.

The strong dip at 438 cm^{-1} is due to the Zn-O stretching vibrations thus confirming that the sample is Zinc Oxide.

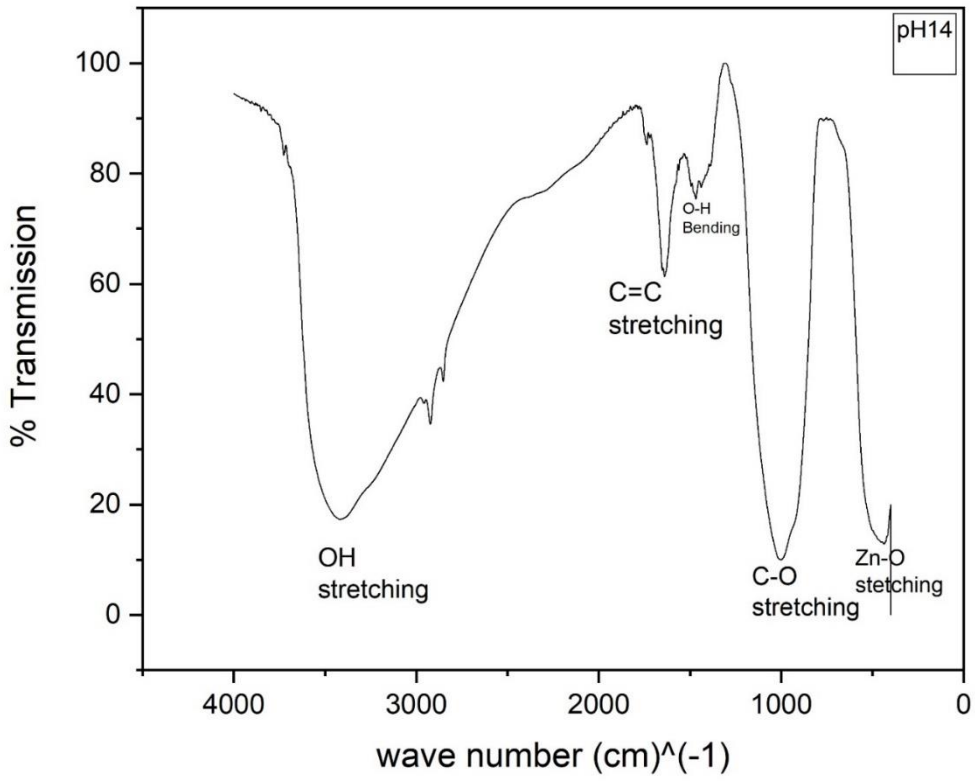

Figure 3. 8 FTIR Spectrum of ZnO Quantum Dots of pH 14

3.2.2. UV – Visible Absorption Spectroscopy

Spectrophotometry is one of the most basic yet most popular Optical Characterization technique, where the absorption and transmission of light by a material is measured for varying energies of incident photons that irradiate the material. The Absorbance of the material as a function of wavelength or energy of the incident photon is recorded. Thus, the method is able

to detect the energies of photons which causes electron transitions within the material, i.e., Band Gap Energies and other transition energies. Here, we have used a Spectrophotometer which excites the material with photons of wavelength ranging from 200 nm to 800 nm. The obtained absorption spectrum is as follows.

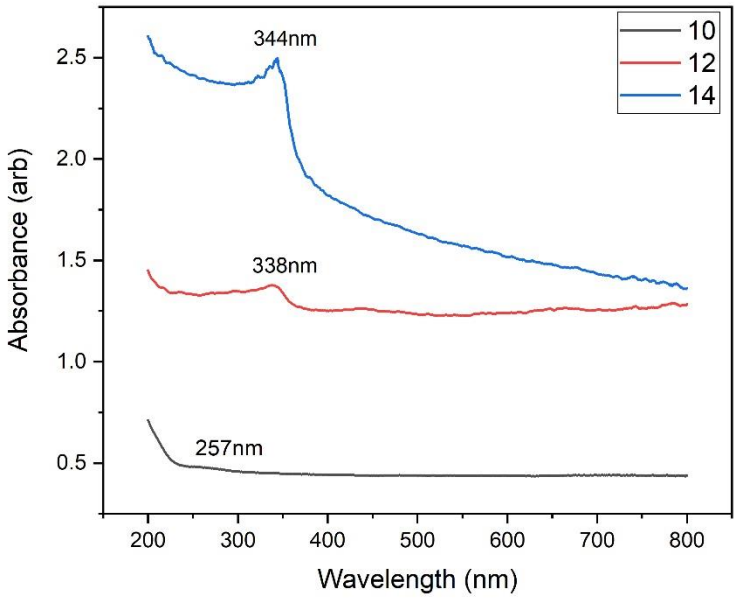

Figure 3. 9 Combined absorption spectrum of pH 10, 12 and 14 ZnO Quantum Dots

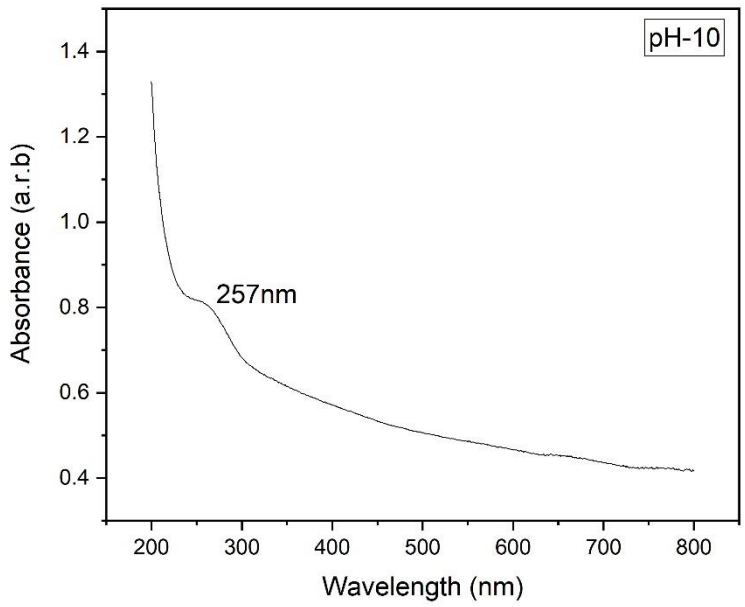

Figure 3. 10 Absorption spectrum of pH 10 ZnO QD in focus

The wavelengths at the beginning of the absorption peaks for pH 10, 12 and 14 respectively are 257 nm, 338 nm and 344 nm, which corresponds to Band Gap Energies 4.824 eV, 3.668 eV and 3.604 eV respectively. A blue shift in band gap energy along with decrease in particle size is observed, which is due to the Quantum Confinement Effects.

As particle size decreases, Quantum Confinement Effects become more prominent. In a Quantum Dot, the electron is confined in all three dimensions ,i.e., the electrons are highly localized. This in turn localizes the energy states , causing the Density of Energy states to be discrete, similar to a series of spikes corresponding to the allowed energy states, This effectively increases the energy gap between the highest energy state within the valence band and the lowest energy state within the conduction band, i.e., Band Gap Energy of the material increases. This shift in energy towards the high energy end of the visible spectrum with decrease in particle size is evident from the Absorption Spectrum of the three samples, further confirming their increase in size with increase in reaction pH.

3.2.3. Photoluminescence Spectroscopy

Photoluminescence Spectroscopy, called PL in short, is another nondestructive materials characterization technique, where luminescence by the excitation of photons is studied. Luminescence is when any material emits energy in the form of light by transition from an excited state to a ground state. If the excitation is caused by a photon, then the phenomenon is Photoluminescence. Photoluminescence can be further divided into Fluorescence and Phosphorescence. The emitted photon has energy less than that of the incident photon, as the electron in the excited state undergoes vibrational relaxations and comes down to a lower energy level, before transitioning back to the ground state along with emitting radiation. This in turn causes the emitted radiation to be of higher wavelength than the incident radiation, known as Stoke’s Shift. The device records intensity of the emitted light as a function of its energy or wavelength. Photoluminescence spectrum can be analyzed to identify Band Gap Energy transitions, fluorescence quenching, impurity energy levels, defects etc.

Photoluminescence spectrum of all three samples (S2) excited with eight different wavelengths of light was recorded. The samples were recorded with 250 nm, 300 nm, 330 nm, 350 nm, 400 nm, 450 nm, 488 nm and 500 nm.

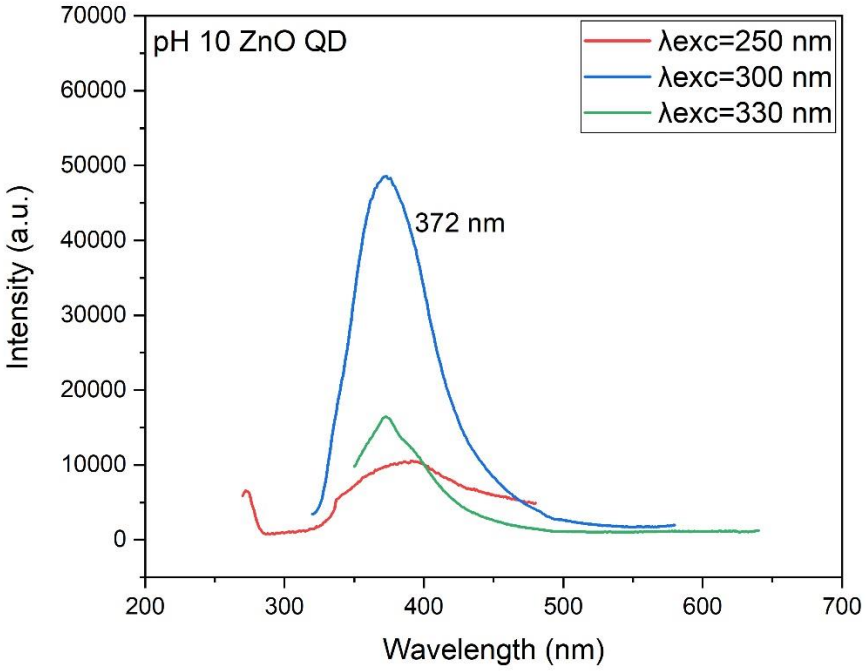

Figure 3. 11 pH 10 ZnO QD excited with photons of energy greater than bandgap energy

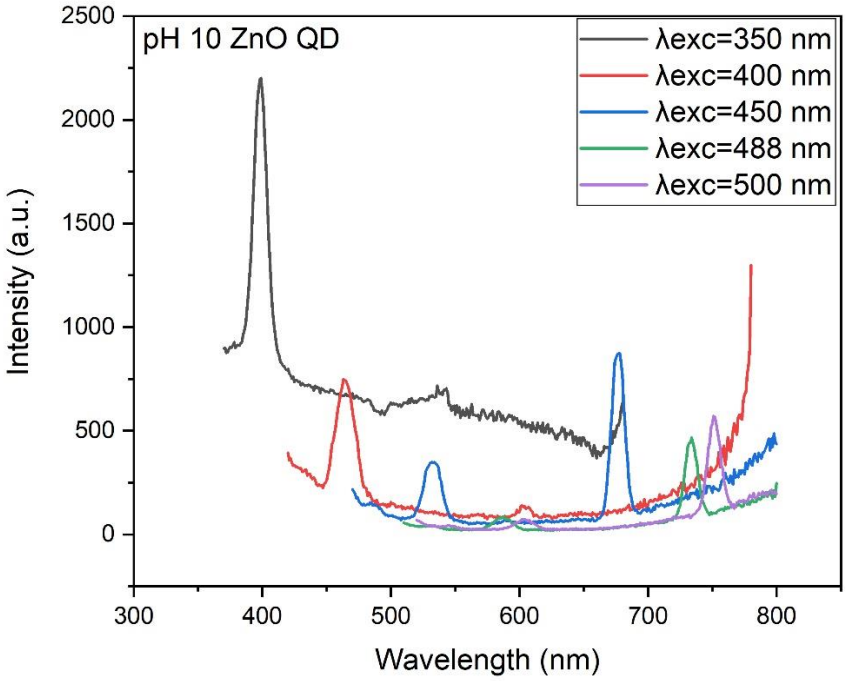

Figure 3. 12 pH 10 ZnO QD excited with photons of energy lesser than bandgap energy

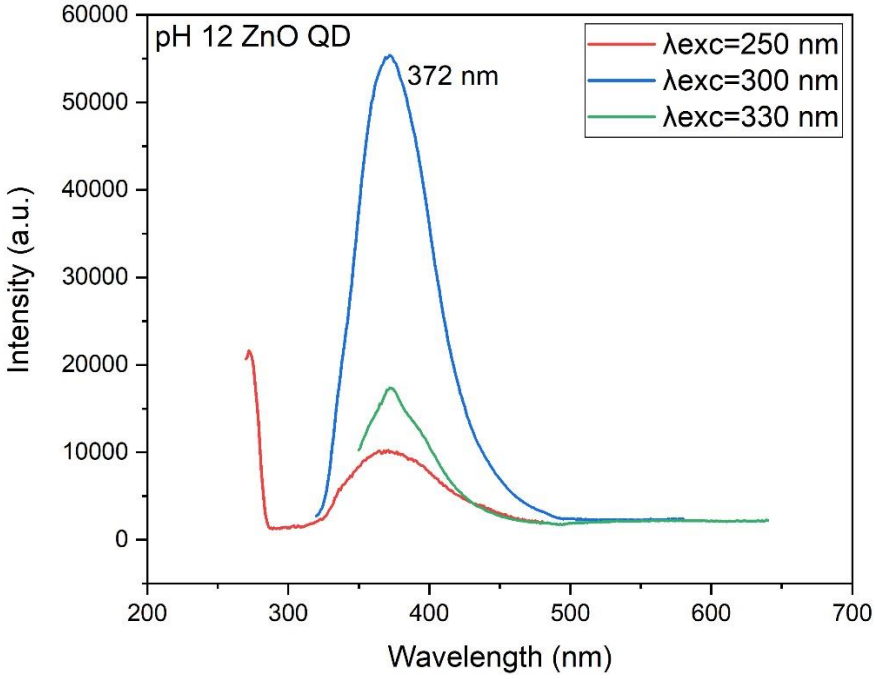

Figure 3. 13 pH 12 ZnO QD excited with photons of energy greater than bandgap energy

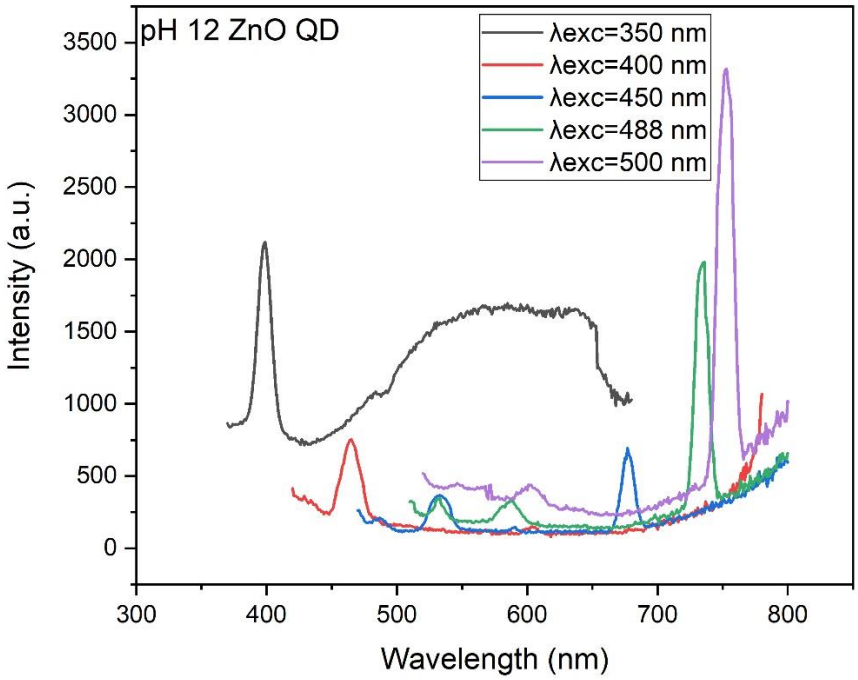

Figure 3. 14 pH 12 ZnO QD excited with photons of energy lesser than bandgap energy

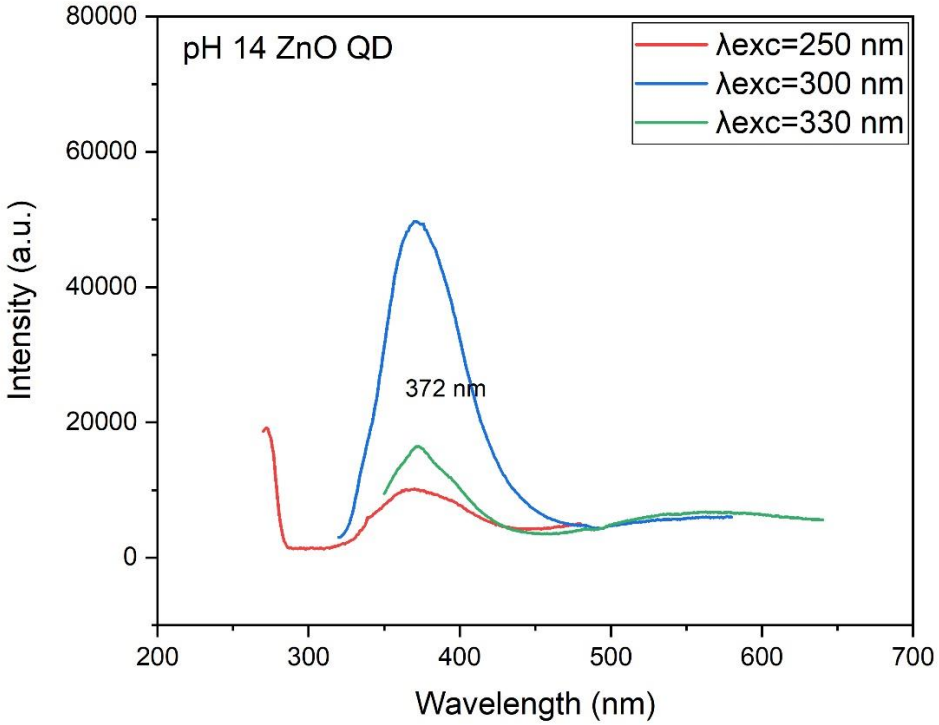

Figure 3. 15 pH 14 ZnO QD excited with photons of energy greater than bandgap energy

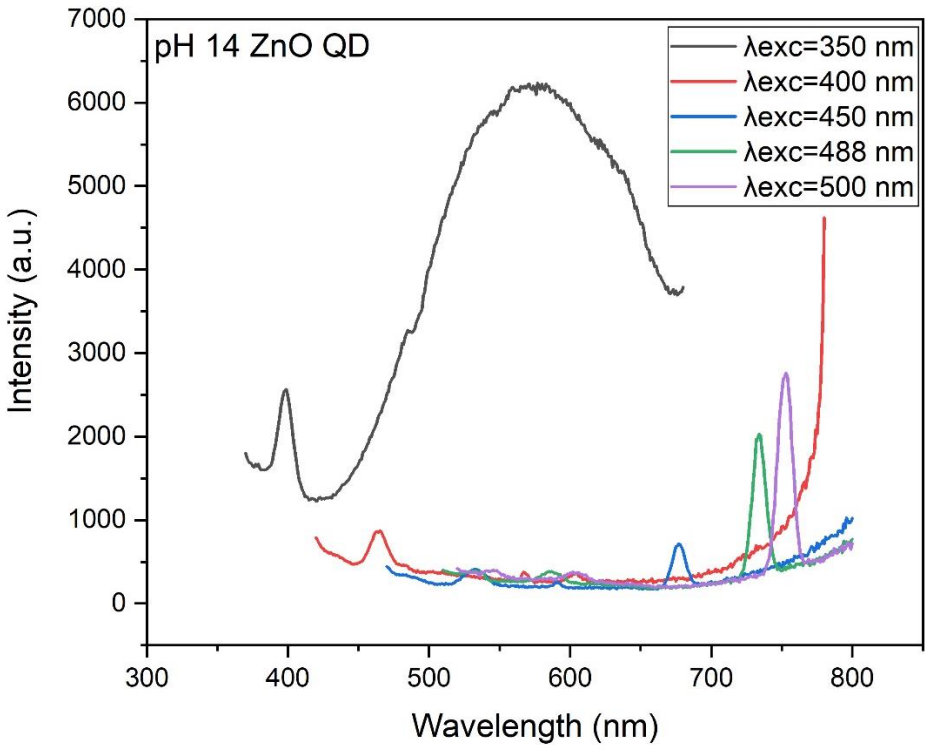

Figure 3. 16 pH 14 ZnO QD excited with photons of energy lesser than bandgap energy

There is a strong emission in the UV region, when excited with photons of energy greater than band gap energy, due to the band edge recombination of free electrons. The optimum excitation wavelength for this emission in UV region to be strongest is, 330 nm. The transition occurs between some energy level within the band gap, but close to the band gap energy, which implies the radiation could be due to exciton recombination. The exciton energy level is slightly lesser than the Band gap energy, and the difference between their energies is equivalent to the exciton binding energy. The energy difference between the emission in the UV region of the Photoluminescence spectrum, and the band gap energy, can be explained by the exciton binding energy that is expected to be greater than that of the bulk counterparts. Zinc Oxide has a high exciton binding energy of about 60 meV at room temperature, and this is supposed to increase with decrease in particle size, as smaller the size of the quantum well, larger is the exciton binding energy. Further, M. Elward et al has reported increase in exciton binding energy with decrease in the size of Quantum Dots in his studies.

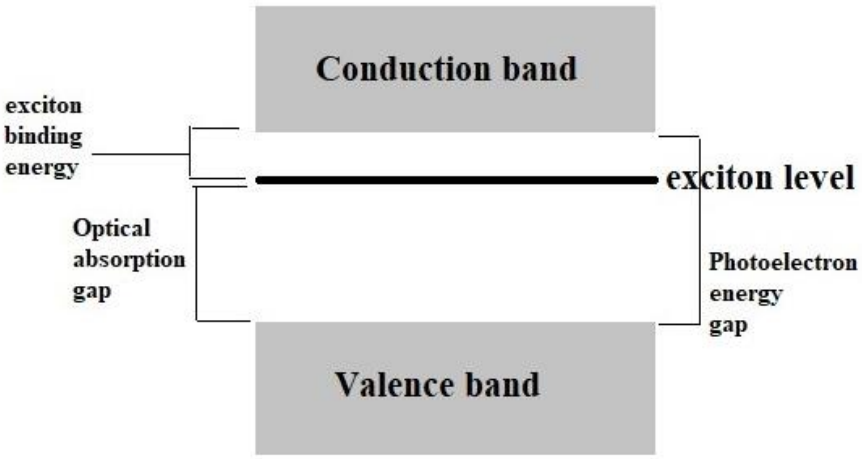

Figure 3. 17 Exciton energy level diagram

Relatively weak emissions in the visible region were observed when excited with photons of energy less than the band gap energy. This indicates the presence of numerous impurity energy levels within the bandgap, to enable these transitions when excited with photons of energy less than that of the bandgap. These trap centers are due to Zinc interstitials or Oxygen Vacancy defects. Deeply trapped electrons and holes within these defect sites has their energy levels lying within the bandgap, and the recombination of these deep trapped carriers causes the visible emission.The exact transition mechanism isn't clear, yet the following picture suggests possible electron hole recombinations causing emission in visible region.

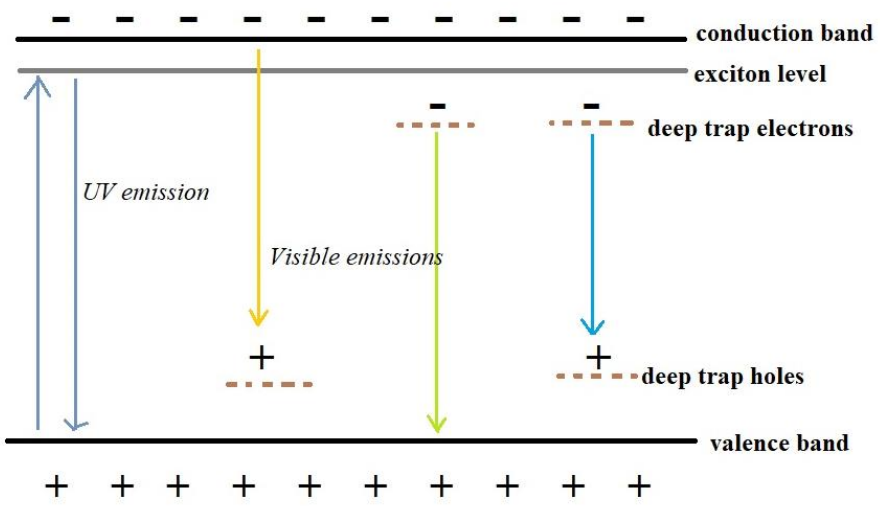

Figure 3. 18 Possible recombinations for visible emission

These visible emissions are found to be tunable with varying excitation wavelengths, which makes the material suitable for various opto-electronic applications.

Chapter 4

PHOTOTHERMAL STUDIES

Abstract

This chapter highlights the thermal diffusivity studies of ZnO QDs using dual beam thermal lens experiment. DPSS CW lasers of wavelengths 488nm and 635nm were used a pump and probe lasers. The experiment was carried for different volume fractions (0 to 14%) of ZnO QDs in water. Initially the sample would be illuminated by the laser sources, following which a mechanical shutter was employed to cut off the pump laser. The sample undergoes nonradiative relaxations by diffusing heat. This was determined by measuring the change in intensity profile of the probe laser at a far field detector. Thermal diffusivity studies of both supernatant and residual parts of the synthesized samples were carried out.

4.1. Introduction

Research on heat transfer applications has been gaining momentum in recent times. One of the important parameters related is the thermal diffusivity which is evident from the equation:

$$K(T) = \alpha(T)\rho(T)C_p(T) \tag{4.1}$$

where K (T) is the thermal conductivity, $\alpha(T)$is the thermal diffusivity of the material, $\rho(T)$ is the density of the material and $Cp(T)$ is the specific heat capacity. Thermal diffusion can be understood as the heat dissipated in a medium. It is important to understand completely mechanism behind thermal diffusion in order to understand heat transfer processes. Thermal Lensing is a sensitive technique which can measure very small changes in refractive index about the beam width of the laser.

4.2. Experimental setup

The thermal diffusivity measurements were carried out using the dual beam thermal lens experiment. The experimental setup employs two laser sources, one of which is called the pump and the other called the probe. It is to be noted that the wavelength of pump laser must be within the absorption range of the sample while that of probe outside this range.

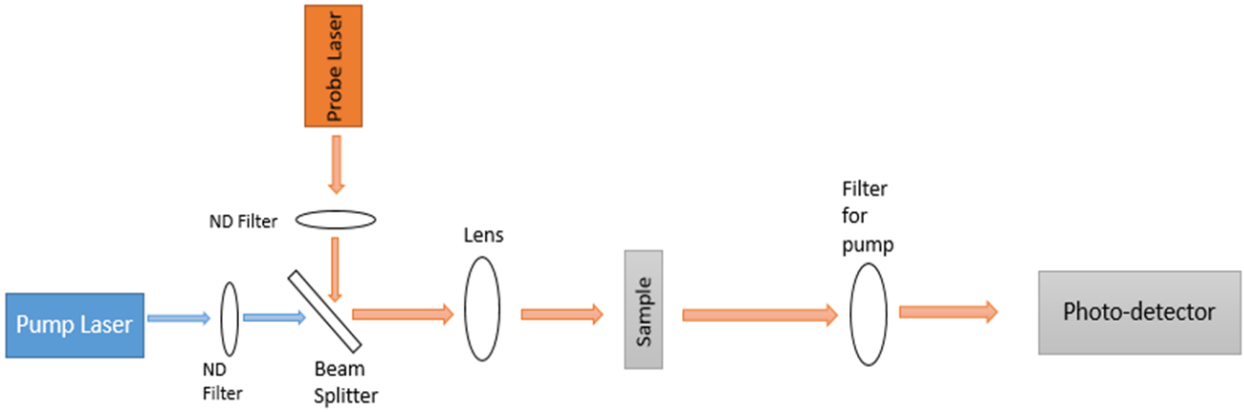

Figure 4. 1 Block diagram of dual beam thermal lens experimental set up

In the present study, DPSS CW laser 488nm (mW) and DPSS CW laser 635nm (mW) was used as the pump and probe lasers respectively. Suitable ND filters are used to reduce spherical aberrations which may be formed due to phase modulation at high laser powers. A mechanical shutter is employed to control the intensity of pump laser. The set up is initially standardized using water whose thermal diffusivity was found to be 1.41×10^{-7} m^2s^{-1} which is in good agreement with the theoretical values. The same setup was used to determine the thermal diffusivity of all three samples of ZnO QDs. The experiment was carried out for various volume fractions (0-14%) of ZnO QDs in water.

Figure 4. 2 The experimental set up of dual beam thermal lens technique

While performing the experiment it is to be kept in mind that the size of the laser beam remains constant while passing through the sample. It is to be made sure that the sample is homogeneous and satisfies Beer Lambert's law.

4.3. Theory

When a sample is irradiated with a laser source, the excited species formed also undergoes nonradioactive relaxation. During the process, the sample absorbs energy which then is converted into heat and hence in turn raises the temperature of the sample. This leads to an expansion of the illuminated medium, therefore the corresponding variation in the refractive index (dn/dT) with temperature of the sample medium becomes negative. Consequently, a diverging lens is formed which aids in spreading the intensity of the pump laser.

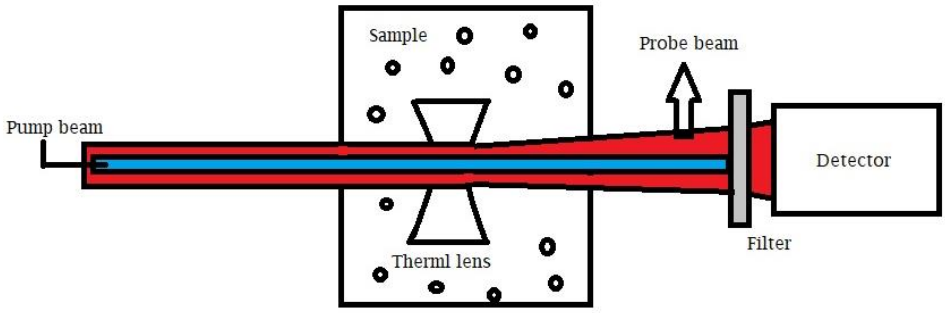

Figure 4. 3 Thermal lens formation

This change in intensity profile of the pump laser is called 'thermal blooming' and is captured using a far filed detector.

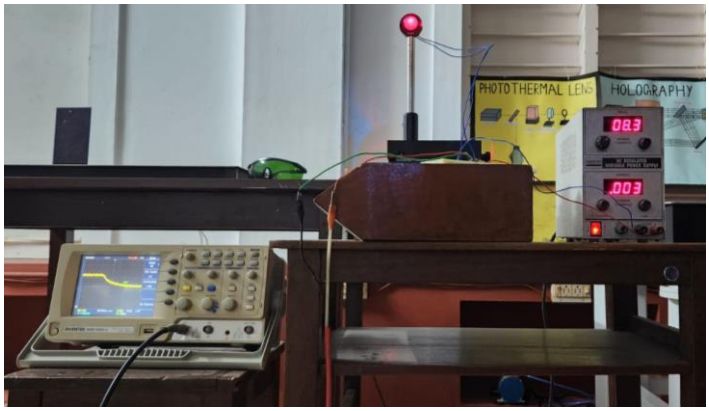

Figure 4. 4 The intensity profile of probe laser recorded using a far field detector onto a DSO.

The photodetector output as shown in fig.4.5. is mathematically fitted to an equation of the form,

$$I(t) = I_0[1 - \frac{\theta}{1+\frac{t_c}{2(t-t_0)}} + \frac{\theta^2}{2(1+\frac{t_c}{2(t-t_0)})^2}]^{-1} \quad (4.2)$$

using MATLAB program which returns θ and t_C values.

Theta is a parameter associated with the thermal power radiated as heat P_{th}

$$\theta = \frac{Pth\left(\frac{dn}{dT}\right)}{\lambda k} \tag{4.3}$$

And t_c is the characteristic time constant for the thermal lens formed to attain a steady state focal length f in the sample medium,

$$t_c = \frac{\omega^2}{4D} \tag{4.4}$$

Where ω refers to the size of the laser beam after passing through the sample medium.

Therefore, the thermal diffusivity D can be determined,

$$D = \frac{\omega^2}{4\ t_c} \tag{4.5}$$

To eliminate possible errors the experimental set up was standardized with water and the thermal diffusivity values of the sample at various volume fractions were determined using the equation,

$$D_{sample} = \frac{D_{water} tc_{water}}{tc_{sample}} \tag{4.6}$$

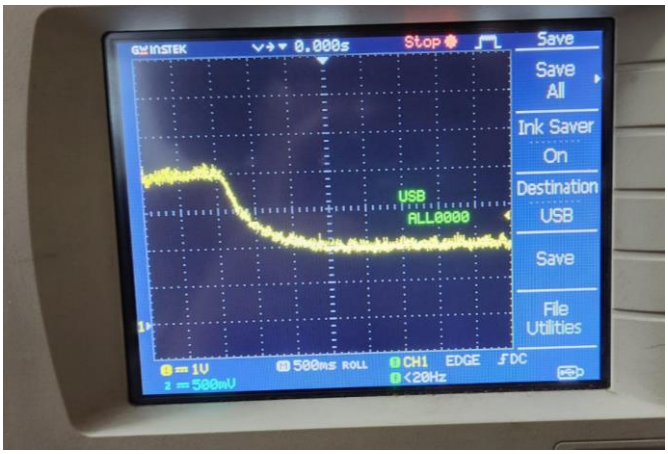

Figure 4. 5 Photodetector output showing decrease in intensity of probe laser owing to thermal blooming

4.4. Analysis

The main mechanism behind the thermal lens technique is thermal conduction, which can be achieved by virtue of three mechanisms.

(a) Brownian motion

ZnO QDs dispersed in water, excited by a laser source causes random motion of particles. These particles enable direct heat transfer while colliding with each other. Increase in volume fraction of the particles inhibits Brownian motion and thereby causes a decrease in thermal diffusivity. This can be attributed to the formation of clusters due to aggregation of the nanoparticles at higher volume fractions.

(b) Near field radiation

It is interesting to note that when the distance between nanoparticles is less their diameters, the heat conduction between them increases as twice or thrice greater than when they are in contact with each other.

(c) Liquid layering

There is a tendency for liquid molecules to form layered structures around solid particles which then act as thermal bridges for the conduction of heat.

Thermal diffusivity studies of the 3 samples were carried out using both supernatant part as well as the sedimented part.

Results of thermal diffusivity study of the supernatant part revealed interesting trends. As shown in fig.4.5, similar trend was observed in all three samples. Initially thermal diffusivity decreases with increase in volume fraction owing to the presence of silica, other impurities and unreacted molecules present in the supernatant part. At increasing concentrations of the sample, Brownian motion is inhibited due to presence of heavier particles, reaches a minimum and then follows a increasing trend with further increase in volume fraction, which can be attributed to near field radiation and liquid layering of nanoparticles.

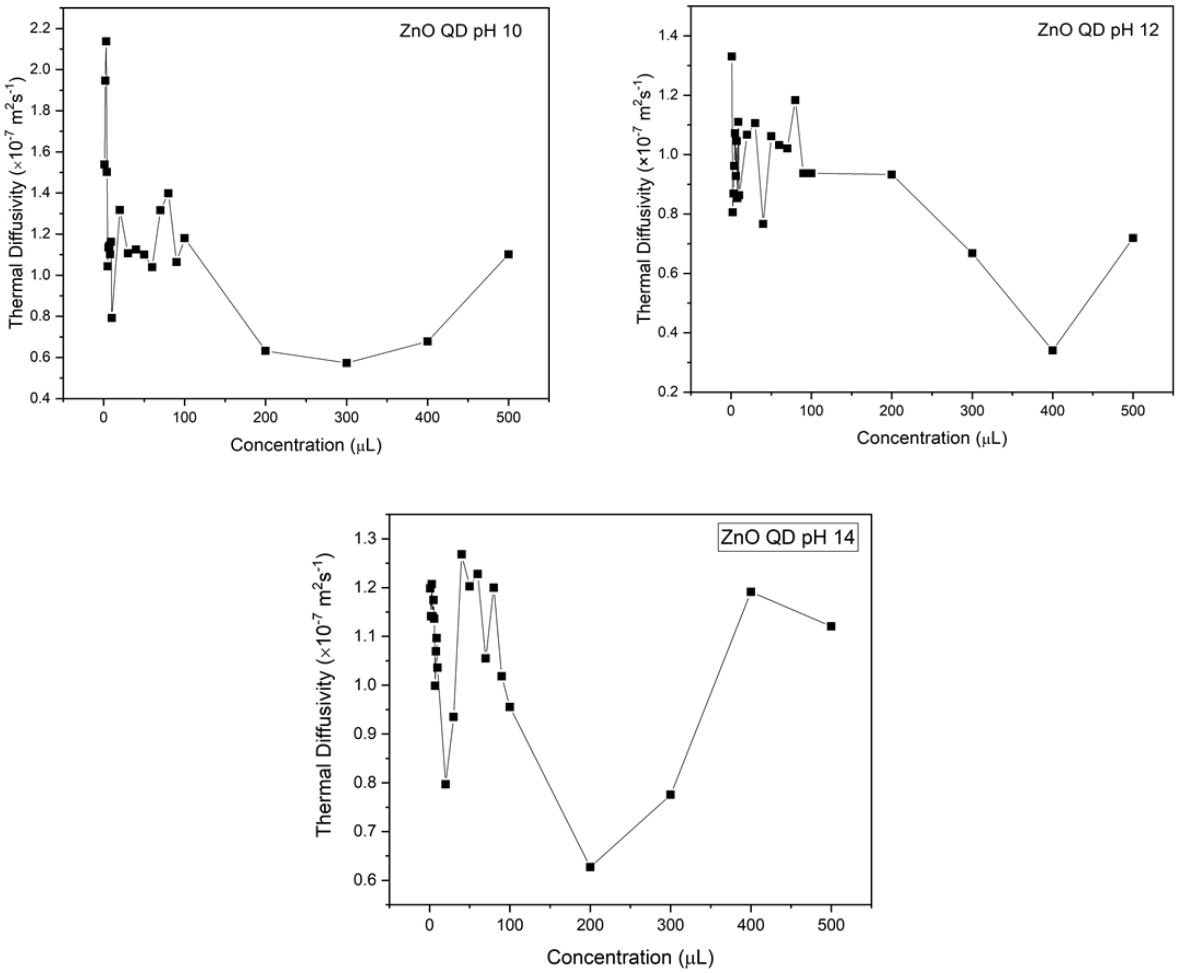

Figure 4. 6 Thermal diffusivity of samples S1 of pH –10,12 and 14

On the other hand, when thermal diffusivity measurements were carried out using the purified sample containing only the ZnO QDs, the results portrayed an increasing trend with volume fraction as shown in fig.4.6.

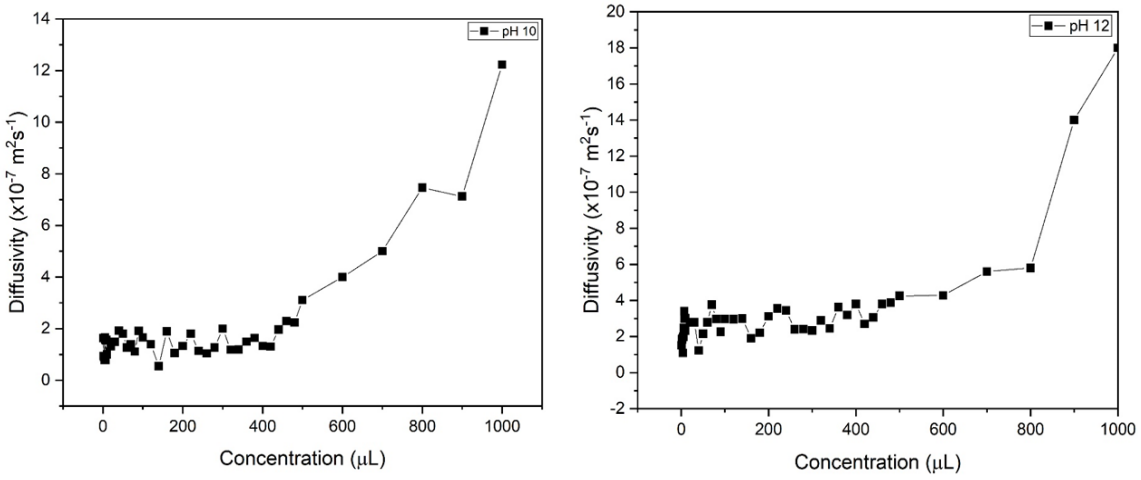

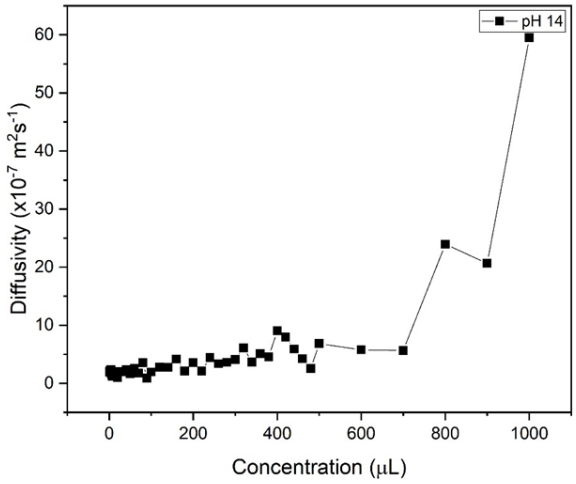

Figure 4. 7 Thermal diffusivity of samples S2 of pH –10,12 and 14

The rising pattern of thermal diffusivity with volume fraction in all three samples can be attributed to liquid layering and near field radiation.

Chapter-5

NON-LINEAR STUDIES

Abstract

Non-linear absorption properties of the Zinc Oxide Quantum Dots are explored. Nonlinear absorption is studied using the open aperture Z-Scan technique. Supernatant part of the colloidal samples showed Saturable absorption for pH 10 and pH 12, and Reverse Saturable absorption for pH 14. The residual sample showed Saturable absorption for all the three reaction pH.

5.1. Introduction

Nonlinear Optics investigates the intensity dependent behavior of light. Materials with nonlinear optical properties interacts with light differently at different intensities of light. Refraction and Absorption properties of the material are found to change with the intensity of light incident on it, which is due to third-order nonlinearities. Lately, third-order nonlinear phenomenon have undergone large amount of studies, and they are much more enhanced in nanomaterials due to Quantum confinement effects.

Nonlinear Optical Phenomenon implies polarization of the material responds nonlinearly to the electric field of light incident on it. Polarization of a medium depends on the electric field as follows.

$$P = \chi_1 E + \chi_2 E^2 + \chi_3 E^3 + \cdots \qquad (5.1)$$

where χ_1 is the linear susceptibility and χ_2, χ_3 etc. are the second and third order nonlinear susceptibilities and so on.

Nonlinear optical response is weak in most medium and hence very high electric field is required to observe Nonlinear phenomenon. Electric fields greater that 10^8 V/m is required, which is possible only through LASERs.

Here, we are investigating Nonlinear Absorption properties of ZnO Quantum Dots using Open Aperture Z-Scan Method.

A material is said to have Nonlinear absorption if it's Absorption Coefficient depends on the intensity of the incident light, at that instant or in the near past. In certain cases, absorption coefficient is reduced or enhanced at higher intensities. The former case is called Saturable Absorption and the latter is Reverse Saturable Absorption. Saturable Absorbers are exploited for Q Switching, Passive Mode Locking etc. in LASERs whereas Reverse Saturable Absorbers find their place in Optical limiting applications.

5.2. Experimental Setup

The method for investigating Nonlinear Absorption of a material is the Open Aperture Z-Scan Method. A laser beam is focused to a point by passing it through a lens and the sample is placed on a translation stage and translated through the optical axis such that it moves across the beam waist. The beam waist will be at the focal point of the lens.The sample will have maximum intensity of light incident on it at the beam waist, where the beam diameter is the smallest and the radiant flux will be maximum. The incident light intensity decreases towards either sides of the beam waist. The transmittance through the sample as it moves through the optical axis is recorded using a Power Detector at the far field. The translation is along the z-axis, hence the name Z-Scan technique.

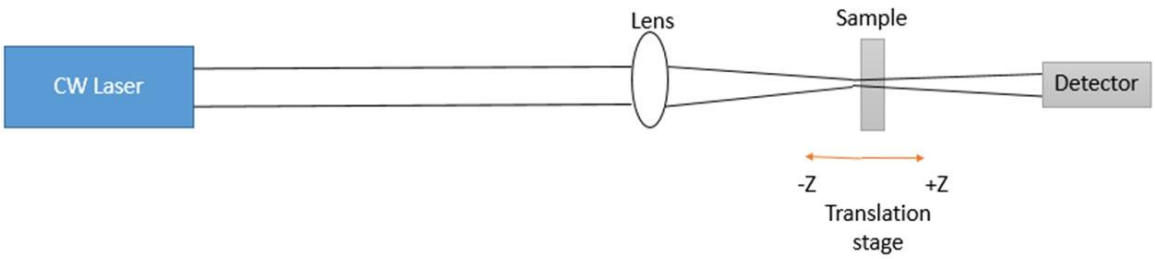

Figure 5. 1 Schematic diagram of Open Aperture Z-Scan technique

Here we've used a 488 nm SAPPHIRE blue LASER as the collimated source of light. The sample was prepared by mixing 0.005 g of the fine powdered sample (S2) in 5 ml of deionized water and ultrasonicating it for 5 minutes. The supernatant sample was taken as it is. The sample was filled in a cuvette of thickness 1 mm and placed on the translation stage. Transmitted power at the far field was recorded as the sample was translated along the beam.

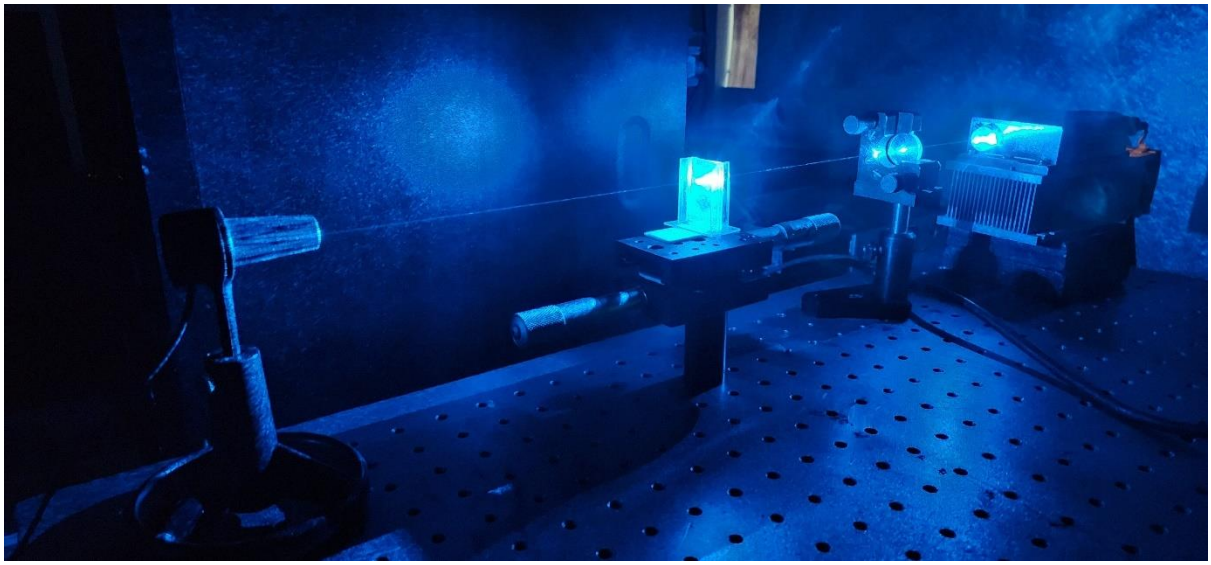

Figure 5. 2 Experimental setup for Open Aperture Z-Scan technique

5.3. Theory

In nonlinear optics, for Reverse Saturable Absorption, nonlinear absorption coefficient α(I), linear absorption coefficient α_0 and Two Photon Absorption Coefficient β are related by the following equation.

$$\alpha(I) = \alpha_0 + \beta(I) \tag{5.2}$$

The distribution of irradiance at the surface of the sample from which the lights exits is given by

$$I_r(z, r, t) = \frac{I(z,r,t)e^{-\alpha L}}{1+\beta^{I(z,r,t)}L_{eff}} \tag{5.3}$$

Where L_{eff} is the effective sample length given by

$$L_{eff} = \frac{1-e^{-\alpha L}}{\alpha} \tag{5.4}$$

where L is the sample length.

Integrating equation 5.3 over limits z and r, total transmitted power is obtained as

$$P(z, t) = P_I(t)e^{-\alpha L}\frac{ln[1+q_0(z,t)]}{q_0(t)} \tag{5.5}$$

Where $q_0 = \frac{\beta I_0(t) L_{eff}}{\left(1+\frac{z^2}{z_0^2}\right)}$ and $P_I(t) = \frac{\pi \omega_0^2 I_0(t)}{2}$ (5.6)

Integrating equation (5.5) over time for a Gaussian pulse gives normalized energy transmittance.

The normalized transmitted energy thus obtained is

$$T_{(z,s=1)} = \frac{1}{\sqrt{\pi q_0(z,0)}} \int_{-a}^{a} ln\left[1 + q_0(z,0)e^{-t^2}\right]dt \quad (5.7)$$

For $|q_0| < 1$, it is expressed as

$$T_{(z,s=1)} = \sum_{m=0}^{a} \frac{[-q_0(z,0)]^m}{(m+1)^{3/2}} \quad (5.8)$$

Where m is an integer. q_0 is obtained by fitting Open Aperture Z-Scan experimental data to equation (5.8)

Then β is obtained from

$$\beta I(z,r,t) L_{eff} = q(z,r,t) \quad (5.9)$$

Imaginary part of third order nonlinear susceptibility is related to β as

$$Im\left(\chi^{(3)}\right) = \frac{\varepsilon_0 n_0^2 c^2 \beta}{\omega} (m^2 V^{-2}) = \frac{n_0^2 c^2 \beta}{240\pi^2 \omega} \quad (5.10)$$

Where ε_0 is permittivity, n_0 is linear refractive index of sample and c is the speed of light.

$\chi^{(3)}$ is expressed in m^2V^{-2}, but is mostly expressed in esu (cgs unit).

$$1\ m^2V^{-2} = 9 \times 10^8 \text{ esu} \quad (5.11)$$

For Saturable Absorption, transmission increases with intensity and absorption decreases with increase in intensity. The absorption coefficient obtained is negative and equation (5.5) fails.

Then we have

$$\alpha(I) = \frac{\alpha_0}{1+\left(\frac{I}{I_S}\right)} \quad (5.12)$$

Substituting equation (5.12) in equation (5.5) and integrating I between the limits I_0 and I_L,

$$ln\left(\frac{I_L}{I_0}\right) = -\alpha_0 L - \left(\frac{I_L - I_0}{I_0}\right) \quad (5.13)$$

Where I_L and I_S are transmission and saturation intensity respectively. Equation (5.13) is numerically solved to obtain I_L. If intensity of excitation is less than I_S, then it is considered to be a third order process and then, $^{-\alpha_0}/_{I_s}$ is the same as nonlinear absorption coefficient β.

5.4. Analysis

The supernatant sample when investigated using Open Aperture Z-Scan Technique gave the following data.

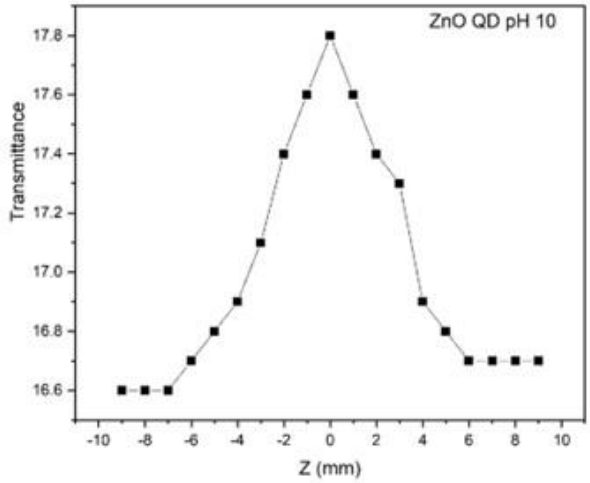

Figure 5. 3 Nonlinear absorption of S1 pH 10 ZnO QD

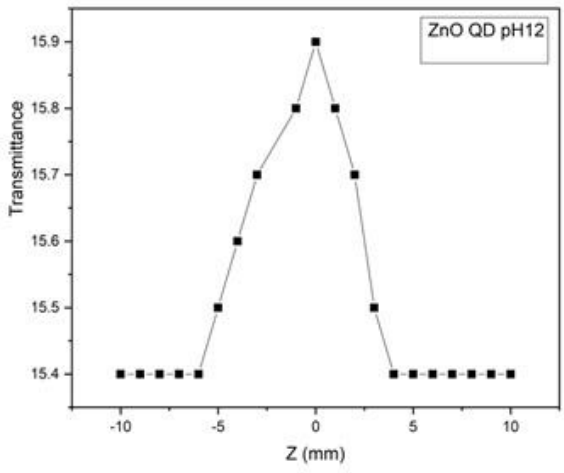

Figure 5. 4 Nonlinear absorption of S1 pH 12 ZnO QD

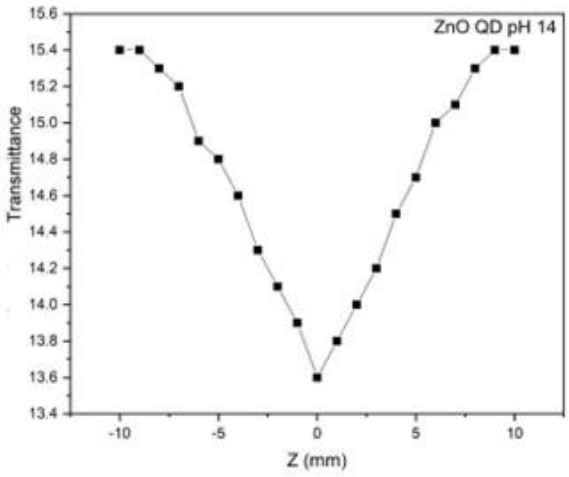

Figure 5. 5 Nonlinear absorption of S1 pH 14 ZnO QD

Samples S1 of pH 10 and 12 are showing Saturable Absorption, i.e., maximum transmittance at maximum intensity. S1 sample of pH 14, on the other hand, showed Reverse Saturable Absorption which is minimum transmittance at maximum intensity.

The S2 samples were dispersed in deionized water at an amount of 0.005 g in 5 ml, and was used to investigate Nonlinear Absorption. The following data was obtained.

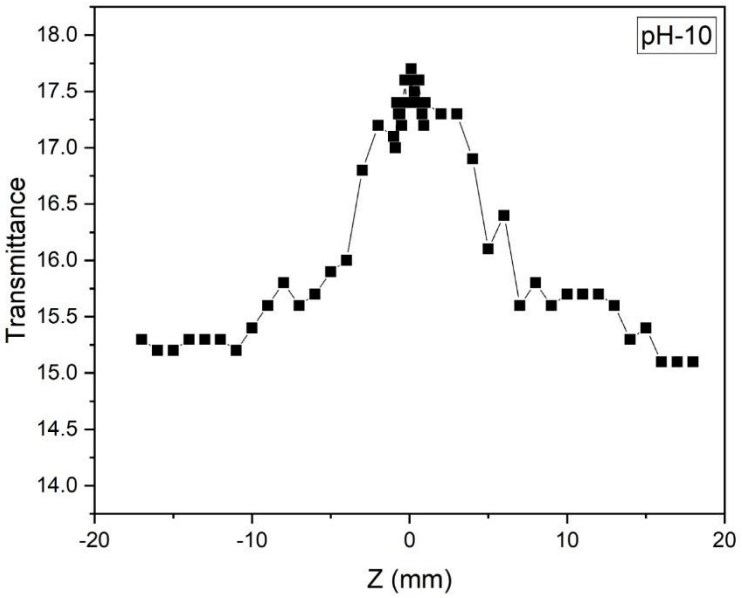

Figure 5. 6 Nonlinear absorption of pH 10 ZnO QD

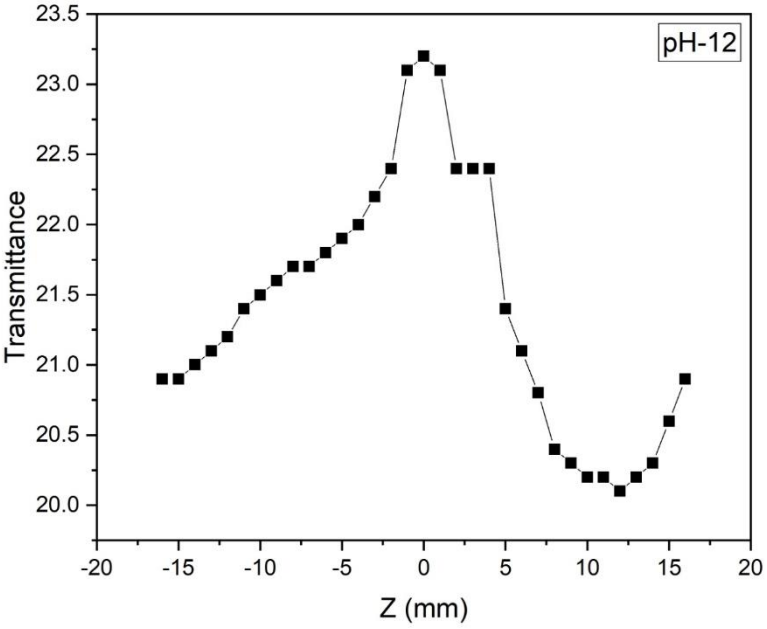

Figure 5. 7 Nonlinear absorption of pH 12 ZnO QD

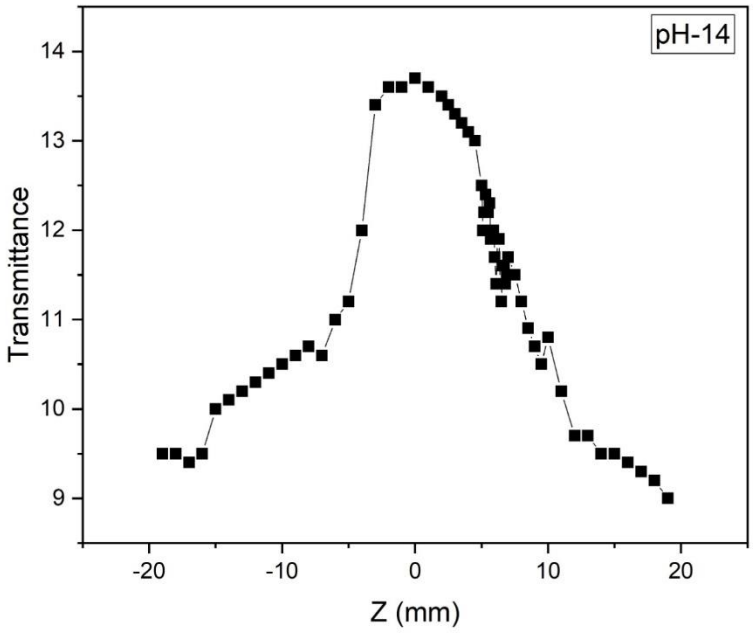

Figure 5. 8 Nonlinear absorption of pH 14 ZnO QD

Here, all the three samples show Saturable Absorption with maximum transmittance at maximum intensity.

Saturable absorption happens when the incident intensity is very high such that the electrons are excited to an upper level at a very high rate such that the ground state soon becomes depleted. Thus the absorption is saturated and does not rise beyond a certain level, causing maximum transmittance. In Reverse Saturable Absorption, at very high intensity, Two Photon Absorption (TPA) and Two Photon induced Excited State Absorption (ESA) may take place if a single photon is not sufficient to overcome the bandgap. In such cases, the absorption is maximized and thus transmittance becomes minimum at maximum intensity.

Chapter-6

CONCLUSION

In this work, ZnO QDs were successfully synthesized using Intermediate sol-gol technique. It was characterized structurally morphologically and optically to confirm the formation of ZnO QDs. High Resolution TEM images revealed the formation of spherical particles of sizes 2.36nm and 4.183nm for ZnO QDs of pH 10 and 14 respectively. It can also be inferred from this characterization, that the size of the QDs have increased with pH owing to the conclusion that addition of more amount of KOH leads to growth of particles leading to the formation larger particle sizes.

This result was further confirmed from the XRD data analysis of the three samples. The XRD pattern revealed peaks which corresponded to the standard values of ZnO. The diffraction planes indicated the hexagonal wurtzite structure of ZnO QDs in all the samples. The approximate crystallite sizes of ZnO QDs of pH-10,12 and 14 were found to be 2.503nm, 5.49nm and 6.42nm, while interplanar spacing was found to be of 0.18nm, 0.202nm and 0.26nm. The lattice parameters and aspect ratios were also calculated which came to be in close approximation to the ideal values. XRD pattern of the supernatant part of the samples were also studied and it revealed amorphous character owing to the presence of Silica, which was used as the capping agent to control particle growth.

Optical characterizations were done to study the interaction of ZnO QDs with light. Absorption spectra revealed a blue shift in the absorption wavelengths and hence the bandgap energy with decrease in particle size which can be attributed to the quantum confinement effects. The photoluminescence spectra showed strong emission in the UV region when excited with lower wavelengths. Strongest emission was observed when excited with wavelength of 330nm which can be attributed to the transitions involving exciton recombinations. Weak emissions were also observed in the visible region when excited with higher wavelengths. The reasons may be the presence of the recombination of electrons and holes in the deeply trapped defect centers. The slight shifts of the emissions peaks in the visible region when excited with higher wavelengths brings forward the tunable nature of ZnO QDs by varying excitation wavelengths and hence suitable in various optoelectronic applications.

FTIR spectrum confirmed the presence of various molecular groups present in the sample.

Thermal diffusivity measurements of S1 samples follow a similar trend. It decreases initially with increase in concentration of the particles reaches a minimum and then increases at higher concentrations. Hence at lower concentrations ZnO QDs can find applications where localized heating is necessary such as in disease treatments to destroy malignant cells without damaging the surrounding healthy cells and tissues. On the other hand, thermal diffusivity of S2 samples showed an increasing trend with concentration, hence can be used as coolants in various devices.

Non-linear optical studies of sample S1 ZnO QDs of pH 14 exhibited reverse saturable absorption make it an excellent material as optical limiters in military applications to protect sensitive organs such as the human eye from intense lasers. Non linear behavior of all other samples portrayed saturable absorption making them useful in passive mode-locking, Q-switching, optoelectronics etc.

Further studies can be undertaken using a closed aperture set up and hence determine the nonlinear absorption coefficient as well as the non-linear refractive index of the material. Nonlinear studies can also be extended with lasers of different wavelengths, as well as with varying the power of the laser source to study the variation in non-linear absorption of the sample with respect to the varying parameters which may find applications in different fields of science and engineering.

REFERENCES

1. https://www.emm-nano.org/what-is-nanoscience-nanotechnology/
2. https://education.nationalgeographic.org/resource/nanotechnology
3. Ramya, M., et al. "Concentration dependent thermo-optic properties of yellow emissive ZnO quantum dots." *Materials Research Express* 6.12 (2019): 126208.
4. Patra, M. K., et al. "Synthesis of stable dispersion of ZnO quantum dots in aqueous medium showing visible emission from bluish green to yellow." *Journal of Luminescence* 129.3 (2009): 320-324.
5. Fu, Ying-Song, et al. "Stable aqueous dispersion of ZnO quantum dots with strong blue emission via simple solution route." *Journal of the American Chemical Society* 129.51 (2007): 16029-16033.
6. Kumar Verma, Awadhesh. "ZnO quantum dots a novel nanomaterial for various applications: Recent advances and challenges." *Indian Journal of Biochemistry and Biophysics (IJBB)* 59.12 (2022): 1190-1198.
7. Cao, H. L., et al. "Shape-and size-controlled synthesis of nanometre ZnO from a simple solution route at room temperature." *Nanotechnology* 17.15 (2006): 3632.
8. Talam, Satyanarayana, Srinivasa Rao Karumuri, and Nagarjuna Gunnam. "Synthesis, characterization, and spectroscopic properties of ZnO nanoparticles." *International Scholarly Research Notices* 2012 (2012).
9. Poul, L., et al. "Synthesis of inorganic compounds (metal, oxide and hydroxide) in polyol medium: A versatile route related to the sol-gel process." *Journal of Sol-Gel Science and Technology* 26.1-3 (2003): 261-265.
10. Soares, J.A., 2014. Introduction to optical characterization of materials. *Practical Materials Characterization*, pp.43-92.
11. https://www.ossila.com/en-in/pages/photoluminescence

12. Van Dijken, A., et al. "Identification of the transition responsible for the visible emission in ZnO using quantum size effects." *Journal of Luminescence* 90.3-4 (2000): 123-128.

13. Van Dijken, A., et al. "The luminescence of nanocrystalline ZnO particles: the mechanism of the ultraviolet and visible emission." *Journal of Luminescence* 87 (2000): 454-456.

14. Zhang, Luyuan, et al. "Origin of visible photoluminescence of ZnO quantum dots: defect-dependent and size-dependent." *The Journal of Physical Chemistry C* 114.21 (2010): 9651-9658.

15. Elward, J.M. and Chakraborty, A., 2013. Effect of dot size on exciton binding energy and electron–hole recombination probability in CdSe quantum dots. *Journal of chemical theory and computation*, *9*(10), pp.4351-4359.

16. Yin, M., et al. "Determination of nonlinear absorption and refraction by single Z-scan method." *Applied Physics B* 70 (2000): 587-591.

17. Walden, Sarah L., et al. "Nonlinear absorption and fluorescence in ZnO and ZnO–Au nanostructures." *Advanced Optical Materials* 4.12 (2016): 2133-2138

18. Ganeev, R. A. "Nonlinear refraction and nonlinear absorption of various media." *Journal of Optics A: Pure and Applied Optics* 7.12 (2005): 717.

19. Chapple, P. B., et al. "Single-beam Z-scan: measurement techniques and analysis." *Journal of Nonlinear Optical Physics & Materials* 6.03 (1997): 251-293.

20. Gu, Bing, et al. "Two-photon-induced excited-state absorption: Theory and experiment." *Applied Physics Letters* 92.9 (2008): 091118.